EUROPEAN ORGANISATION FOR NUCLEAR RESEARCH

CERN-PPE /93-185
19.10.1993.

PHOTO- AND HADRO- PRODUCTION OF $\phi(1020)$, $K^*(892)^0$ AND $\overline{K}^*(892)^0$ MESONS IN THE ENERGY RANGE 65 TO 175 GEV

The OMEGA Photon Collaboration, CERN, Geneva, Switzerland

R. J. Apsimon[5], M. Atkinson[3], M. Baake[1], L. S. Bagdasarian[7], D. Barberis[2], T. J. Brodbeck[4], N. Brook[3], T. Charity[4], A. B. Clegg[4], P. Coyle[3], S. Danaher[6], S. Danagulian[7], M. Davenport[2], B. Dickinson[3], B. Diekmann[1], A. Donnachie[3], A. T. Doyle[3], J. Eades[2], R. J. Ellison[3], F. Fiedler[1], P. S. Flower[5], J. M. Foster[3], W. Galbraith[6], P. I. Galumian[7], C. Gapp[1], F. Gebert[1], G. Hallewell[5], K. Heinloth[1], R. C. W. Henderson[4], M. T. Hickman[4], K. C. Hoeger[1], R. P. Hofmann[1], A. Holzkamp[1], S. Holzkamp[1], R. E. Hughes-Jones[3], M. Ibbotson[3], H. P. Jakob[1], D. Joseph[1], N. R. Keemer[4], J. Kingler[1], G. Körsgen[1], S. D. Kolya[3], G. D. Lafferty[3], H. McCann[3], R. McClatchey[2], C. McManus[3], D. Mercer[3], J. A. G. Morris[5], J. V. Morris[5], D. Newton[4], A. O'Connor[4], R. Oedingen[1], A. G. Oganesian[7], P. J. Ottewell[3], C. N. Paterson[5], E. Paul[1], D. Reid[3], H. Rotscheidt[1], P. H. Sharp[5], S. Soeldner-Rembold[1], N. A. Thacker[6], L. Thompson[6], R. J. Thompson[3], J. Waterhouse[3], A. S. Weigend[1], G. W. Wilson[4].

[1] Physikalisches Institut, Universität, Nussallee 12, D-5300 Bonn, Germany
[2] CERN, CH-1211 Geneva 23, Switzerland
[3] Department of Physics, The University, Manchester M13 9PL, England
[4] School of Physics and Materials, Lancaster University, Lancaster LA1 4YB, England
[5] Rutherford-Appleton Laboratory, Chilton, Didcot, Oxon OX11 0QX, England
[6] Department of Physics, University of Sheffield, Sheffield S3 7RH, England
[7] Yerevan Physics Institute, Markavion St. 2, SU-375 036 Yerevan, Armenia.

Abstract

Inclusive production of ϕ, K^{*0}, and $\overline{K^{*0}}$ mesons has been measured in γp, $\pi^{\pm}$p and $K^{\pm}$p collisions at beam energies of 65 GeV < E_γ < 175 GeV and $E_{\pi/K} = 80$ and 140 GeV. Cross sections have been determined over the range $0 < x_F < 1.0$ and $0 < p_T < 1.8$ GeV/c. Emphasis is put on the comparison of cross sections for different projectiles as a function of x_F so as to study the effects of common quarks between the beam particle and the detected ϕ, K^{*0} or $\overline{K^{*0}}$. The data are compared with a parton fusion model. Many features of the data are well explained. In detail the strange quark appears to carry a large fraction of the kaon momentum and the contribution of the valence quarks from the proton is small.

Z. Phys. C (to be published)

1 Introduction

Measurements have been made with the OMEGA spectrometer at the CERN-SPS (experiment WA69) of the 15 reactions:

$$\begin{array}{lll} \gamma p \to \phi X, \ K^{*0}X \text{ or } \overline{K^{*0}}X & & 65 \text{ GeV} < E_\gamma < 175 \text{ GeV}, \\ \pi^{\pm} p \to \phi X, \ K^{*0}X \text{ or } \overline{K^{*0}}X & & E_\pi = 80 \text{ GeV and } E_\pi = 140 \text{ GeV}, \\ K^{\pm} p \to \phi X, \ K^{*0}X \text{ or } \overline{K^{*0}}X & & E_K = 80 \text{ GeV and } E_K = 140 \text{ GeV}, \end{array}$$

where X is a hadronic system, containing at least two charged tracks detected in the spectrometer, produced together with the ϕ, K^{*0} or $\overline{K^{*0}}$.

Inclusive ϕ and $K^{*0}/\ \overline{K^{*0}}$ production have been studied by many previous workers eg [1], [2], [3], [4], [5], [6], [7] and give information on reaction mechanisms with the signature of a strange quark in the final state. The parton fusion model [8], which assumes that the meson is produced by picking up one parton from the beam (sea or valence quark or gluon) and the other from the target, can give a good description of inclusive meson production with photon and hadron beams over a large range in x_F. This has been shown, for example, for the ρ^0 meson [9] at low x_F and low p_T. The resulting invariant cross section $(2E^*/\sqrt{s})d\sigma/dx_F$ is determined by a convolution of pairs of structure functions taking account of all allowed combinations of valence and sea quarks and gluons. Final states with an s quark are particularly fruitful for such a study because this quark comes from the sea for pion beams and dominantly from the projectile for kaon beams. Regge exchange is expected to contribute to ϕ and $K^{*0}/\overline{K^{*0}}$ production at large x_F. The availability from this experiment of data from both initial hadron charges is particularly valuable for quark fusion model studies since the asymmetries associated with the quark content of the proton can be studied. A recent discussion of these areas is given by [10].

Section 2 gives an outline of the experimental setup, trigger, and data reduction and section 3 describes the evaluation of cross sections. Section 4 gives the results while section 5 provides a discussion of them in terms of models. A summary is given in section 6.

2 The experiment, trigger, and data reduction

The CERN Omega Photon experimental layout is shown in figure 1. The photon beam was obtained as electron bremsstrahlung from a radiator target and individual photon energies were determined by measuring the incoming and outgoing electron and cover the range 65 GeV$<E_\gamma <$ 175 GeV. The hadron beams provided particles of energies 80 and 140 GeV and of both charges. The π/K ratio was measured, and adjusted to a value of 2:1 in the trigger, by means of differential Cherenkov counters (CEDARs) in the beamline. The interactions took place in a 60 cm long liquid hydrogen target. A system of multi-wire proportional chambers and drift chambers and the OMEGA magnetic field of 1.8 T served to reconstruct and determine the momentum of charged secondaries. A Ring Image Cherenkov Counter (RICH) with discriminating power in the momentum range from 5 to 80 GeV/c and a Transition Radiation Detector (TRAD) covering mainly momenta greater than 80 GeV/c were used to separate $K^{\pm}$ from $\pi^{\pm}$.

In the RICH, Cherenkov photons were emitted from charged tracks in a 5 m deep C_2F_6 radiator and reflected by a 7 m by 4 m spherical mirror system at the rear of the detector on to its focal plane sited at the front. Thus the photons arrive on a ring whose diameter

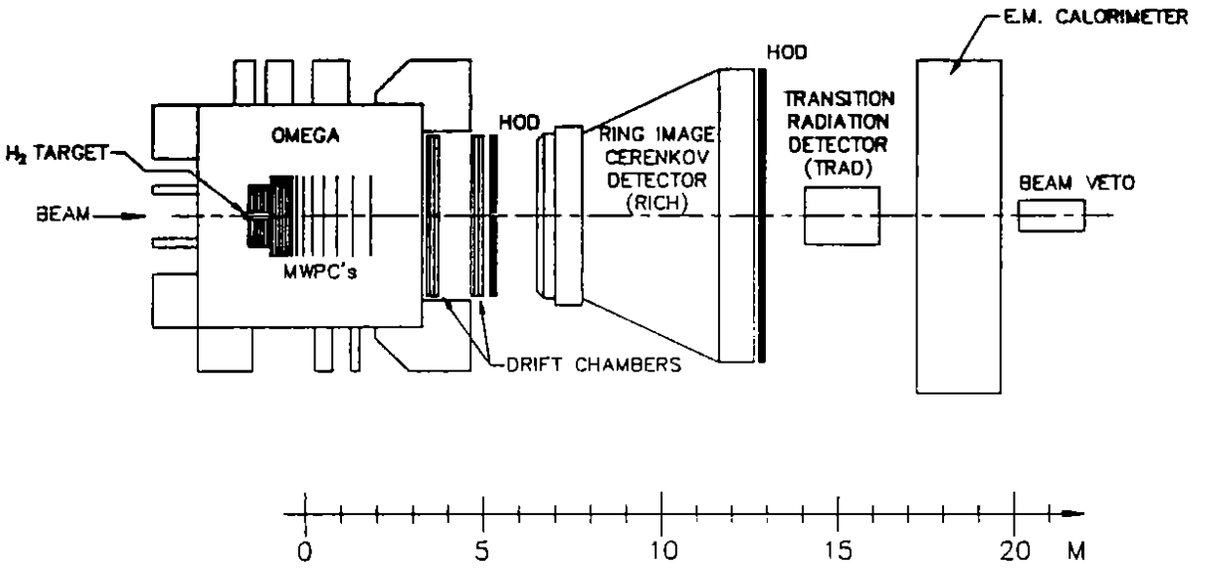

Figure 1: Schematic layout of the experiment

depends on their emission angle and hence on the particle velocity. They are detected by time projection chambers with quartz entrance windows and a TMAE admixture in the chamber gas so as to be sensitive to the wavelength of the Cherenkov photons. A detailed description of the device is given elsewhere [11]. The TRAD detector is a 12-fold sandwich array consisting of a (transition) radiator stack made of polypropylene fibers interleaved with drift chamber planes. The drift chambers were filled with xenon to detect the transition radiation as well as the original track. The zone hit by the primary photon beam was deactivated. A full description is given in [12].

The trigger was tuned to be as similar as possible for photon and hadron beam data with the rejection of e^+e^- pairs in γp data being the most stringent constraint. The trigger required a signal from an endcap scintillation counter behind the hydrogen target, at least one charged track outside the median plane of the spectrometer, together with vetos on either (a) electrons or positrons hitting the median strip of an electromagnetic calorimeter [13], or (b) double bremsstrahlung causing substantial energy deposition in a rear beam veto counter. The spectrometer track was defined by a correlated coincidence between two split hodoscope arrays in front and at the rear of the RICH. This split excluded from the trigger dip angles less than about ± 5 mrad out of the e^+e^- contaminated median plane. The only other differences in the trigger for the two beam types were the additional requirement of a signal from a tagged beam electron in the γp data, or of a signal from the CEDAR's in the hadron data and the removal of the beam veto requirement for hadron beam data. For genuine hadronic final states these requirements correspond to a rather weak restriction, so that for both beam types a trigger on most of the total cross section was provided.

A total of 20×10^6 photon induced triggers and 24×10^6 hadron induced triggers were recorded. The latter consisted of four parts according to beam energies and charge polarities (4×10^6 each at ± 80 GeV and 8×10^6 each at ± 140 GeV). More detail is given in [14].

The raw data were passed through an event reconstruction program, TRIDENT [15], responsible for pattern recognition and track and vertex reconstruction, while particle

identification from the RICH and TRAD were added in a second program. The trigger left a significant contamination of electromagnetic pairs in the photon beam data and these were eliminated after pattern recognition by requiring at least four charged tracks from a single vertex together with TRAD and electromagnetic calorimeter information consistent with hadronic final states. To achieve uniformity, this cut was applied to all data. It leads to some reduction in the fraction of the total cross section measured. Cuts were applied on the vertex position, beam particle reconstruction, and distance of closest approach of a track to the vertex.

3 Particle identification, measurement of ϕ and K^{*0}, and determination of efficiencies

3.1 Particle identification

The particle identification weight P_i of the RICH for a charged track i (where $i = e^{\pm}, \mu^{\pm}, \pi^{\pm}, K^{\pm}$ or $p/\overline{p}$ and $\sum_i P_i = 1$) depends on the diameter of, and the number of photons in, the corresponding ring. All particles with a weight P_K greater than a pre-determined minimum (P_K^{min}) were taken to be kaons. The value of this cut was optimized by studying the misidentification probabilities. Study of the signal to background ratio for the diffractive reaction $\gamma p \rightarrow \phi p$ in the range 65 GeV $< E_\gamma <$ 175 GeV showed that the misidentification increased rapidly if $P_K^{min} < 0.4$ but that any higher value gave a substantial loss of correct identification without substantial further gains in correct assignments. Thus a value of $P_K^{min} = 0.4$ was used throughout. For the TRAD a similar procedure yielded $P_K^{min} = 0.5$.

Three methods were used to evaluate the efficiencies for correct particle identification by the RICH and TRAD. The first method used exclusively produced ϕ's to identify the kaon and required one kaon to be identified with high probability by the RICH or TRAD. The efficiency for the identification of the other kaon with the RICH or TRAD is then

$$\epsilon^{\pm} = \frac{\text{number of } K^{\pm} \text{ identified by RICH or TRAD as } K^{\pm}}{\text{number of } K^{\pm} \text{ actually entering RICH or TRAD}}.$$

The second method used the subset of inclusive ϕ production where the ϕ signal is clearly visible in the overall two particle mass spectra (i.e. at high x_F in $K^{\pm}$ induced data). Then

$$\epsilon^{\pm} = \frac{\text{number of } \phi \text{ mesons with } K^{\pm} \text{ identified}}{\text{number of } \phi \text{ mesons without } K^{\pm} \text{ identification}}.$$

The above methods only give accurate information at higher K momenta, and to improve the accuracy for lower momenta a third method was used. For the ϕ meson both kaons are very close in momentum due to the small Q value; hence the efficiency for the identification of both kaons from the ϕ decay $\approx \epsilon^+(p)\ \epsilon^-(p)$ (where p is half the ϕ momentum). The ϕ can be fitted in inclusive mass spectra separately for cases where both the K^+ and K^-, or only the K^+, or only the K^-, were identified. Hence a simultaneous fit to the data was used to find the values of ϵ^+ and ϵ^-.

Figure 2 shows resulting efficiencies for K^+ (the data for K^- are almost identical) for (a) photon induced ϕ production and (b) kaon induced ϕ production. The figure indicates that results from method (1) (full circles) are in good agreement with those obtained from (2) (open diamonds) and the more general approach (3) (open circles).

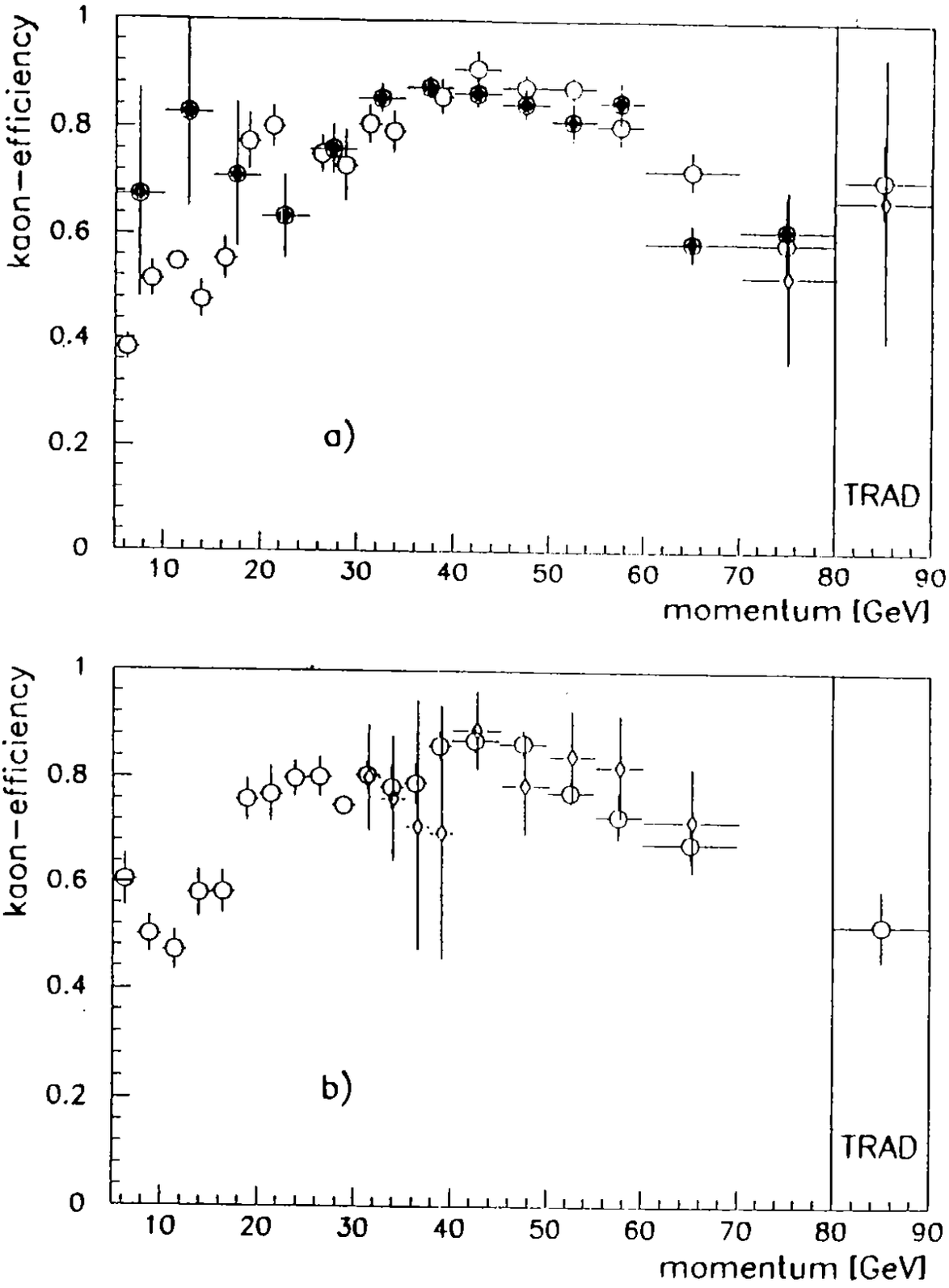

Figure 2: Kaon efficiency as a function of track momentum for positive kaons: (a) photon induced data, (b) kaon induced data; the different symbols refer to different methods of the determination (see text).

3.2 Evaluation of acceptances

Various event generators were used to provide input samples for the acceptance calculation: LUCIFER, LUCVDM, LULOPT [16] and HERWIG [17]. The simulated ϕ and $K^{*0}/\overline{K^{*0}}$ mesons were processed through a simulation of the experimental set-up, and through the event reconstruction. The acceptance was then defined as the ratio of number of mesons surviving to the number generated and was found to vary smoothly as a function of x_F and p_T. An example of the acceptance is shown on figure 3 which is for ϕ-photoproduction with $E_\gamma < 110$ GeV. The statistical errors are negligible except at large x_F and p_T. The decrease in the acceptance at large x_F and low p_T is mainly due to the influence of the e^+e^- veto in the trigger. All generators gave competely consistent results and - to maximise statistics - data from the different generators were added. All experimental results have been corrected using these acceptances.

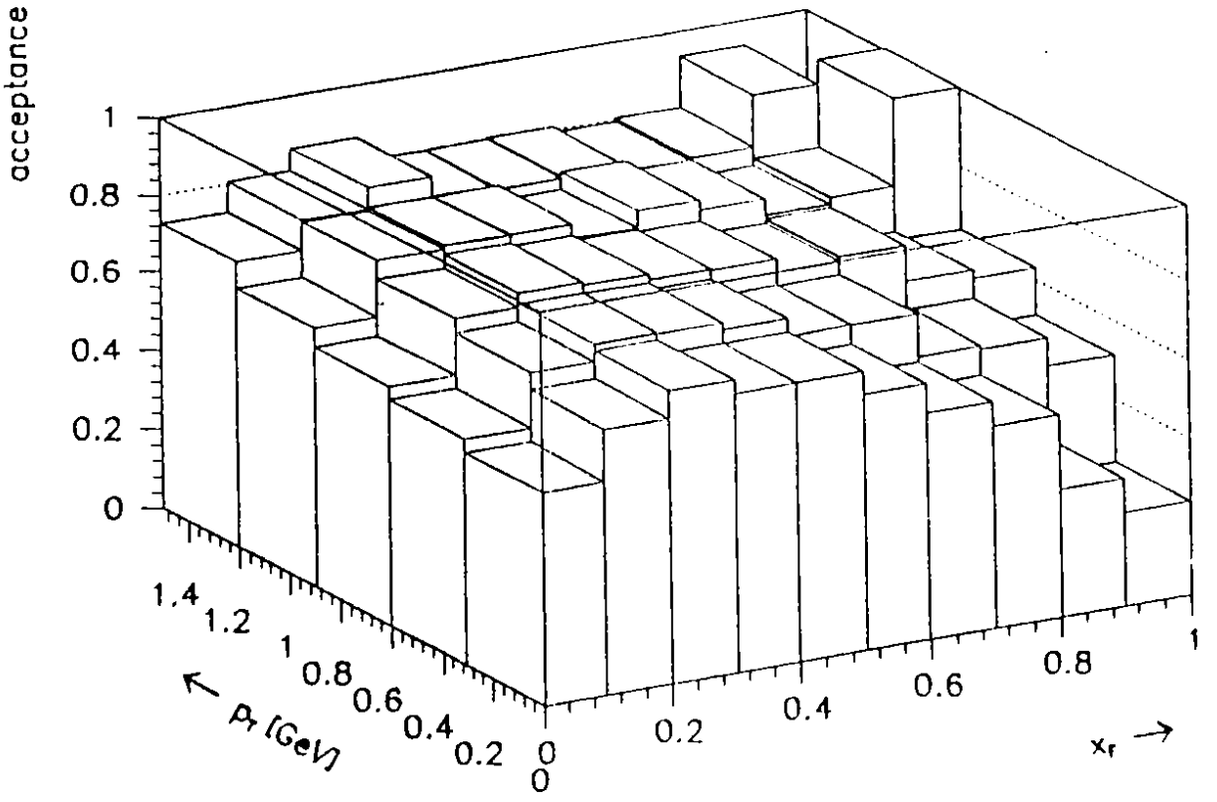

Figure 3: Acceptance for $\gamma p \to \phi X$ for $E_\gamma < 110$ GeV as a function of x_F and p_T.

3.3 Measurement of resonance intensities in mass spectra

Invariant masses were calculated for all pairs of oppositely charged tracks in an event and the resultant mass spectra fitted with the sums of the resonance (using a relativistic Breit-Wigner function - see for example [9]), the reflection of resonances in other channels due to particle misidentification, and a background. The standard PDG [18] values have been used for masses and widths (ϕ: $m = 1.0194$ GeV, and $\Gamma = 0.0044$ GeV; K^{*0}, $\overline{K^{*0}}$: $m = 0.8961$ GeV and $\Gamma = 0.0498$ GeV). These widths were convoluted with experimental resolutions (see below). The parameterization of the background was identical to the one used in [9] and [19]:

$$BG(m; p_4, p_5, p_6, p_7) = p_4(m - m_{thr})^{p_5} \exp(-p_6 m - p_7 m^2).$$

The second factor ensures that the combinatorial background vanishes at threshold.

Summing up all contributions results in

$$\tilde{F}(m) = p_1 BW_\phi(m) + p_2 Refl_{\mathrm{K}^*,\mathrm{KK}}(m) + p_3 Refl_{\rho^0,\mathrm{KK}}(m) + BG(m; p_4, p_5, p_6)$$

for the $\mathrm{K}^+\mathrm{K}^-$ mass plot, and

$$\tilde{F}(m) = p_1 BW_{\mathrm{K}^*}(m) + p_2 Refl_{\phi,\mathrm{K}\pi}(m) + p_3 Refl_{\rho^0,\mathrm{K}\pi}(m) + BG(m; p_4, p_5, p_6, p_7)$$

for the $\mathrm{K}^\pm\pi^\mp$ mass plot. $Refl_{x,y}$ is the reflection of particle x in spectrum y. An additional quadratic (cubic) term in m for the background of the $\mathrm{K}^+\mathrm{K}^-$ ($\mathrm{K}^\pm\pi^\mp$) spectrum yields neither a significant improvement of the χ^2 nor a significant change of the p_1 value.

In order to fold in the experimental resolutions a scatter plot of $\sigma(m_{\mathrm{inv}})$ vs. m_{inv} (the invariant mass of the pairs of detected mesons) was constructed for a given energy range and reaction. $\sigma(m_{\mathrm{inv}})$ was calculated by error propagation from the errors on the track momenta given by the track reconstruction program. For the KK case it was found that for the mean value,

$$\overline{\sigma(m_{\mathrm{KK}})} = \overline{\sigma(m_\phi)} \cdot \sqrt{\frac{m_{\mathrm{KK}} - 2m_{\mathrm{K}}}{m_\phi - 2m_{\mathrm{K}}}}$$

is a good description for all beams and energies. The $\sigma(m)$ distribution for a given m_{inv} was used to evaluate a resolution function $G(\sigma(m), m_{\mathrm{inv}})$ as a weighted sum of gaussian distributions of width $\sigma(m)$. The total fit-function was then

$$F(m) = \int_{m-\delta}^{m+\delta} G(m - m'; m')\tilde{F}(m')dm' \,.$$

The value of δ was chosen so that the contribution to the integration outside of the limits was negligible. Figure 4 shows an example of a fit obtained using the above method for the experimental resolution after subtraction of the background.

3.4 Normalization of cross sections and errors

There are several systematic errors in the evaluation of cross sections: a 10% normalization uncertainty in the intensity of each beam (which is increased by beam veto counter errors to 15% for the photon beam), a 10% error in acceptance calculations and a 5% / 10% error due to the errors in the experimental resolution for the K^{*0}/ϕ respectively.

The relative normalization between negative and positive hadron data is important and the systematic error on this was reduced by taking the number of measured events per beam particle and the inelastic cross sections (as quoted by [18]) in positive and negative beams. The assumption was made that the partial cross section for giving at least four detected charged tracks was the same proportion of the total inelastic cross section for each of the two opposite charges. The correction was chosen so that the average cross sections remained the same. The individual raw cross sections had to be changed by about 10% for each of the two hadron beam charges. The relative positive to negative beam normalization after this correction was tested by measuring the ratios of inelastic ρ^0 production for the different charged beams which were found to be consistent with unity for both beam types and energies. Internal checks within this data also suggested that the final normalization was reliable to a few percent.

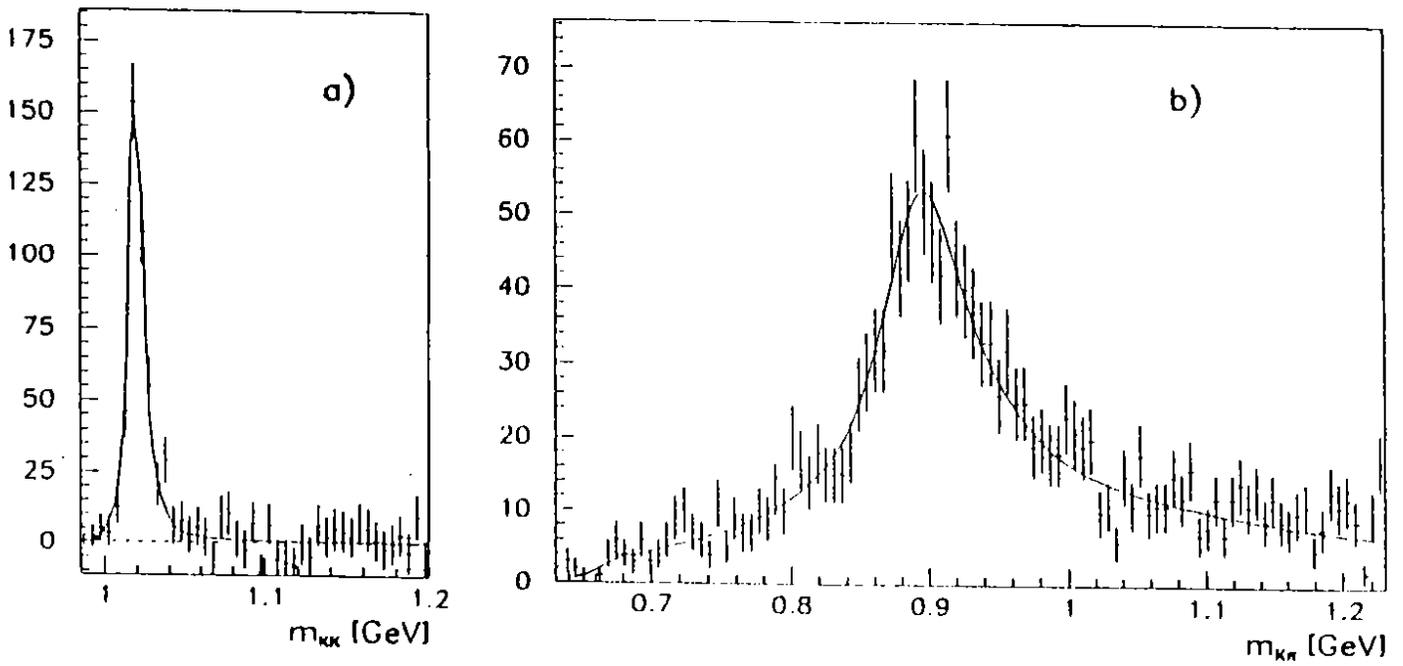

Figure 4: Mass plots for high energy data. (a) shows the ϕ (K^+ induced data, $0.2 < x_F < 0.4$, $0.3 < p_T < 0.6$ GeV/c) fitted with a Breit-Wigner function with nominal values for mass and width convoluted with the resolution function, after subtraction of background and reflections. (b) is the $K^+\pi^-$ mass spectrum (K^+ induced data, $0.8 < x_F < 0.9$, $0.3 < p_T < 0.6$ GeV/c) with a Breit-Wigner K^{*0} but with background and reflections included.

4 Experimental results

4.1 ϕ production

Tables 1 to 3 give the measured cross sections $d^2\sigma/(dx_F dp_T)$ for ϕ production in photon, pion and kaon beam data. Data are quoted for $0.0 < x_F < 1.0$ in bins of 0.1 and for $0 < p_T < 1.5$ GeV/c in 0.3 GeV/c bins. Throughout the paper 'low' energy means 65 GeV $< E_\gamma <$ 110 GeV for γ data and 80 GeV for hadron data and 'high' energy means 110 GeV $< E_\gamma <$ 175 GeV for γ data and 140 GeV for hadron data. A dash indicates either that large corrections prevented the evaluation of a reliable error or the bin had too few events to make a measurement possible. The statistical errors quoted are those given by MINUIT [20] for the resonance intensities in a given mass distribution[1]; additional systematic errors have been discussed above. It is important to note that overall cross sections can only be compared indirectly with previous work since the requirement of two additional detected charged particles causes some loss ($\approx$ 20%) from the total inelastic cross section. This experiment and other published work are in satisfactory agreement within the significant errors of each. (The same argument leads to similar agreement for ρ^0 production [9].) The invariant cross sections show no significant variation with the energy of the projectile.

		$x_F \longrightarrow$									
		0.0-0.1	0.1-0.2	0.2-0.3	0.3-0.4	0.4-0.5	0.5-0.6	0.6-0.7	0.7-0.8	0.8-0.9	0.9-1.0
γ_{low} p_T [GeV/c] $\downarrow$	0.0-0.3	–	1.35 ±0.30	0.83 ±0.18	0.35 ±0.10	0.38 ±0.08	0.31 ±0.07	0.24 ±0.07	0.22 ±0.07	0.40 ±0.07	0.26 ±0.08
	0.3-0.6	–	2.43 ±0.48	1.14 ±0.19	1.24 ±0.16	0.66 ±0.09	0.54 ±0.10	0.44 ±0.09	0.53 ±0.05	0.55 ±0.10	0.50 ±0.06
	0.6-0.9	–	1.66 ±0.32	1.05 ±0.16	0.47 ±0.14	0.63 ±0.08	0.49 ±0.06	0.29 ±0.07	0.27 ±0.08	0.46 ±0.05	0.36 ±0.08
	0.9-1.2	–	0.59 ±0.17	0.48 ±0.11	0.31 ±0.10	0.24 ±0.07	0.16 ±0.05	0.19 ±0.05	0.21 ±0.05	0.18 ±0.03	0.04 ±0.01
	1.2-1.5	–	0.16 ±0.05	0.16 ±0.05	0.05 ±0.02	0.17 ±0.05	0.02 ±0.01	0.06 ±0.02	0.04 ±0.01	0.04 ±0.01	0.05 ±0.02
γ_{high}	0.0-0.3	1.95 ±0.57	1.04 ±0.32	0.84 ±0.25	0.59 ±0.16	0.29 ±0.09	0.25 ±0.08	0.38 ±0.08	0.24 ±0.07	0.24 ±0.07	1.14 ±0.33
	0.3-0.6	2.60 ±0.77	2.64 ±0.22	1.11 ±0.25	0.85 ±0.14	0.78 ±0.11	0.55 ±0.08	0.49 ±0.10	0.43 ±0.09	0.71 ±0.09	0.82 ±0.21
	0.6-0.9	1.59 ±0.48	1.28 ±0.28	0.68 ±0.19	0.78 ±0.15	0.57 ±0.08	0.37 ±0.08	0.34 ±0.10	0.29 ±0.06	0.29 ±0.04	0.33 ±0.04
	0.9-1.2	0.41 ±0.13	0.56 ±0.18	0.54 ±0.16	0.40 ±0.09	0.27 ±0.08	0.20 ±0.04	0.19 ±0.06	0.18 ±0.05	0.25 ±0.07	0.06 ±0.02
	1.2-1.5	0.30 ±0.09	0.12 ±0.04	0.09 ±0.03	0.07 ±0.02	0.08 ±0.03	0.10 ±0.02	0.08 ±0.02	0.05 ±0.02	0.04 ±0.01	0.04 ±0.01

Table 1: Differential cross sections $d^2\sigma/(dx_F dp_T)$ (in μb/GeV/c) for photon induced ϕ production in the range of $p_T < 1.5$ GeV/c and $0.1 < x_F < 1.0$ for low and $0.0 < x_F < 1.0$ for high beam energy. The errors listed are purely statistical.

The gross features of inclusive meson production from photon beams are known to be described by the vector dominance model over a wide range of x_F and p_T. This has been shown for instance in the data on inclusive production of high-p_T mesons [14], in energy flow distributions [21] and in the inclusive production of ρ^0's [9] and π^0's [13] from this experiment and ϕ's from a related earlier experiment [22]; it can also be tested here. Figure 5 shows

$$\frac{1}{R} = \frac{d\sigma/dx_F(hp \to \phi X)}{d\sigma/dx_F(\gamma p \to \phi X)}$$

[1]MIGRAD errors are quoted but a sample was checked using MINOS and showed not more than 20% differences.

		$x_F \longrightarrow$						
		0.0-0.1	0.1-0.2	0.2-0.3	0.3-0.4	0.4-0.5	0.5-0.6	0.6-0.7
π^+_{low} p_T [GeV/c] ↓	0.0-0.3	–	0.18 ± 0.05	0.14 ± 0.04	0.07 ± 0.02	0.03 ± 0.01	0.03 ± 0.01	–
	0.3-0.6	–	0.34 ± 0.10	0.25 ± 0.08	0.08 ± 0.03	0.04 ± 0.01	0.02 ± 0.01	0.02 ± 0.01
	0.6-0.9	–	0.28 ± 0.06	0.13 ± 0.04	0.04 ± 0.01	0.04 ± 0.02	0.04 ± 0.01	0.02 ± 0.00
	0.9-1.2	–	0.12 ± 0.04	0.05 ± 0.02	0.03 ± 0.01	0.03 ± 0.01	0.01 ± 0.00	0.01 ± 0.00
	1.2-1.5	–	0.04 ± 0.02	0.03 ± 0.01	0.02 ± 0.01	0.01 ± 0.01	–	–
π^+_{high}	0.0-0.3	0.49 ± 0.15	0.17 ± 0.06	0.12 ± 0.02	0.02 ± 0.01	0.01 ± 0.00	0.02 ± 0.01	0.02 ± 0.01
	0.3-0.6	0.57 ± 0.18	0.29 ± 0.09	0.19 ± 0.06	0.10 ± 0.03	0.04 ± 0.01	0.03 ± 0.01	0.04 ± 0.01
	0.6-0.9	0.31 ± 0.09	0.19 ± 0.06	0.17 ± 0.03	0.07 ± 0.01	0.02 ± 0.01	0.05 ± 0.01	0.02 ± 0.01
	0.9-1.2	0.13 ± 0.05	0.10 ± 0.03	0.06 ± 0.02	0.04 ± 0.01	0.01 ± 0.00	0.02 ± 0.00	0.01 ± 0.00
	1.2-1.5	0.06 ± 0.02	0.04 ± 0.02	0.04 ± 0.01	0.02 ± 0.01	0.01 ± 0.00	0.01 ± 0.00	–
π^-_{low}	0.0-0.3	–	0.23 ± 0.07	0.19 ± 0.06	0.02 ± 0.01	0.03 ± 0.01	0.02 ± 0.01	–
	0.3-0.6	–	0.43 ± 0.12	0.25 ± 0.08	0.09 ± 0.03	0.06 ± 0.02	0.03 ± 0.01	0.02 ± 0.01
	0.6-0.9	–	0.33 ± 0.10	0.06 ± 0.02	0.03 ± 0.01	0.03 ± 0.01	0.02 ± 0.01	0.02 ± 0.01
	0.9-1.2	–	0.09 ± 0.02	0.08 ± 0.02	0.04 ± 0.01	0.04 ± 0.01	0.01 ± 0.00	–
	1.2-1.5		0.04 ± 0.02	0.02 ± 0.01	0.02 ± 0.01	–	–	–
π^-_{high}	0.0-0.3	0.41 ± 0.12	0.14 ± 0.03	0.09 ± 0.03	0.03 ± 0.01	0.02 ± 0.01	0.01 ± 0.00	0.03 ± 0.01
	0.3-0.6	0.38 ± 0.10	0.29 ± 0.04	0.10 ± 0.03	0.06 ± 0.02	0.05 ± 0.02	0.04 ± 0.02	0.03 ± 0.01
	0.6-0.9	0.33 ± 0.08	0.24 ± 0.08	0.11 ± 0.03	0.05 ± 0.02	0.03 ± 0.01	0.01 ± 0.00	0.01 ± 0.00
	0.9-1.2	0.18 ± 0.05	0.06 ± 0.01	0.05 ± 0.02	0.02 ± 0.01	0.02 ± 0.01	0.01 ± 0.00	0.01 ± 0.00
	1.2-1.5	0.05 ± 0.02	0.03 ± 0.01	0.03 ± 0.01	0.02 ± 0.01	0.02 ± 0.01	–	–

Table 2: Differential cross sections $d^2\sigma/(dx_F dp_T)$ (in mb/GeV/c) for pion induced ϕ production in the range of $p_T < 1.5$ GeV/c and $0.1 < x_F < 0.7$ for low and $0.0 < x_F < 0.7$ for high beam energy. The errors listed are purely statistical and an entry 0.00 indicates a statistical error of < 0.005.

		$x_F \longrightarrow$									
		0.0-0.1	0.1-0.2	0.2-0.3	0.3-0.4	0.4-0.5	0.5-0.6	0.6-0.7	0.7-0.8	0.8-0.9	0.9-1.0
K^+_{low} p_T [GeV/c] ↓	0.0-0.3	–	0.65 ± 0.21	0.22 ± 0.07	0.21 ± 0.06	0.14 ± 0.04	0.15 ± 0.04	0.12 ± 0.04	0.05 ± 0.02	0.12 ± 0.04	0.08 ± 0.04
	0.3-0.6	–	0.92 ± 0.27	0.48 ± 0.14	0.40 ± 0.10	0.37 ± 0.07	0.32 ± 0.06	0.32 ± 0.04	0.21 ± 0.04	0.13 ± 0.04	0.04 ± 0.02
	0.6-0.9	–	0.37 ± 0.11	0.43 ± 0.13	0.22 ± 0.07	0.26 ± 0.08	0.28 ± 0.04	0.17 ± 0.05	0.08 ± 0.03	0.04 ± 0.02	–
	0.9-1.2	–	0.21 ± 0.06	0.17 ± 0.05	0.10 ± 0.03	0.17 ± 0.04	0.04 ± 0.02	0.07 ± 0.03	0.08 ± 0.03	–	–
	1.2-1.5	–	0.10 ± 0.04	0.07 ± 0.03	0.04 ± 0.02	0.04 ± 0.02	0.03 ± 0.01	0.03 ± 0.01	–	–	–
K^+_{high}	0.0-0.3	0.36 ± 0.10	0.31 ± 0.09	0.21 ± 0.06	0.25 ± 0.04	0.20 ± 0.05	0.25 ± 0.05	0.21 ± 0.05	0.14 ± 0.03	0.11 ± 0.03	0.03 ± 0.01
	0.3-0.6	0.86 ± 0.16	0.47 ± 0.14	0.41 ± 0.05	0.52 ± 0.09	0.37 ± 0.07	0.35 ± 0.06	0.23 ± 0.03	0.23 ± 0.05	0.15 ± 0.04	0.04 ± 0.01
	0.6-0.9	0.42 ± 0.13	0.31 ± 0.07	0.30 ± 0.05	0.30 ± 0.03	0.21 ± 0.02	0.26 ± 0.03	0.21 ± 0.03	0.17 ± 0.02	0.14 ± 0.04	0.02 ± 0.01
	0.9-1.2	0.23 ± 0.06	0.20 ± 0.06	0.19 ± 0.05	0.17 ± 0.04	0.12 ± 0.03	0.10 ± 0.03	0.09 ± 0.02	0.08 ± 0.02	0.02 ± 0.01	–
	1.2-1.5	0.10 ± 0.04	0.09 ± 0.03	0.06 ± 0.02	0.05 ± 0.02	0.03 ± 0.01	0.04 ± 0.01	0.02 ± 0.01	0.02 ± 0.01	–	–
K^-_{low}	0.0-0.3	–	0.56 ± 0.17	0.17 ± 0.04	0.09 ± 0.03	0.14 ± 0.04	0.27 ± 0.08	0.13 ± 0.03	0.21 ± 0.06	0.09 ± 0.03	–
	0.3-0.6	–	0.77 ± 0.22	0.85 ± 0.25	0.54 ± 0.11	0.46 ± 0.10	0.38 ± 0.09	0.35 ± 0.06	0.20 ± 0.07	0.14 ± 0.04	–
	0.6-0.9	–	0.51 ± 0.14	0.51 ± 0.14	0.36 ± 0.11	0.13 ± 0.03	0.21 ± 0.07	0.27 ± 0.07	0.12 ± 0.03	0.16 ± 0.04	0.06 ± 0.02
	0.9-1.2	–	0.13 ± 0.03	0.28 ± 0.09	0.20 ± 0.06	0.03 ± 0.02	0.08 ± 0.02	0.07 ± 0.02	0.04 ± 0.02	–	–
	1.2-1.5	–	0.10 ± 0.03	0.06 ± 0.02	0.02 ± 0.01	0.06 ± 0.02	0.04 ± 0.02	0.01 ± 0.01	–	–	–
K^-_{high}	0.0-0.3	0.34 ± 0.09	0.27 ± 0.09	0.19 ± 0.05	0.14 ± 0.04	0.19 ± 0.04	0.27 ± 0.06	0.12 ± 0.02	0.10 ± 0.03	0.11 ± 0.03	0.08 ± 0.03
	0.3-0.6	0.54 ± 0.14	0.30 ± 0.09	0.38 ± 0.11	0.27 ± 0.06	0.32 ± 0.06	0.33 ± 0.04	0.44 ± 0.05	0.19 ± 0.05	0.19 ± 0.03	0.02 ± 0.01
	0.6-0.9	0.58 ± 0.18	0.23 ± 0.06	0.26 ± 0.06	0.28 ± 0.06	0.22 ± 0.05	0.20 ± 0.05	0.20 ± 0.03	0.20 ± 0.04	0.14 ± 0.03	0.02 ± 0.01
	0.9-1.2	0.16 ± 0.05	0.22 ± 0.06	0.13 ± 0.04	0.12 ± 0.03	0.12 ± 0.03	0.08 ± 0.02	0.06 ± 0.02	0.08 ± 0.02	0.03 ± 0.01	–
	1.2-1.5	0.10 ± 0.03	0.03 ± 0.01	0.03 ± 0.01	0.02 ± 0.01	0.05 ± 0.02	0.02 ± 0.01	0.01 ± 0.00	0.02 ± 0.01	–	–

Table 3: Differential cross sections $d^2\sigma/(dx_F dp_T)$ (in mb/GeV/c) for kaon induced ϕ production in the range of $p_T < 1.5$ GeV/c and $0.1 < x_F < 1.0$ for low and $0.0 < x_F < 1.0$ for high beam energy. The errors listed are purely statistical and an entry 0.00 indicates a statistical error < 0.005.

for both energy intervals where "h" is a $\frac{2}{3}\pi + \frac{1}{3}$K mixture of hadron data to simulate the strange and non-strange quark content of a VDM-type photon. The data at low x_F give $1/R \approx 220$ which is consistent with expectations although at large x_F quasi-diffractive ϕ photoproduction gives an additional contribution and so causes a decrease in 1/R (see below).

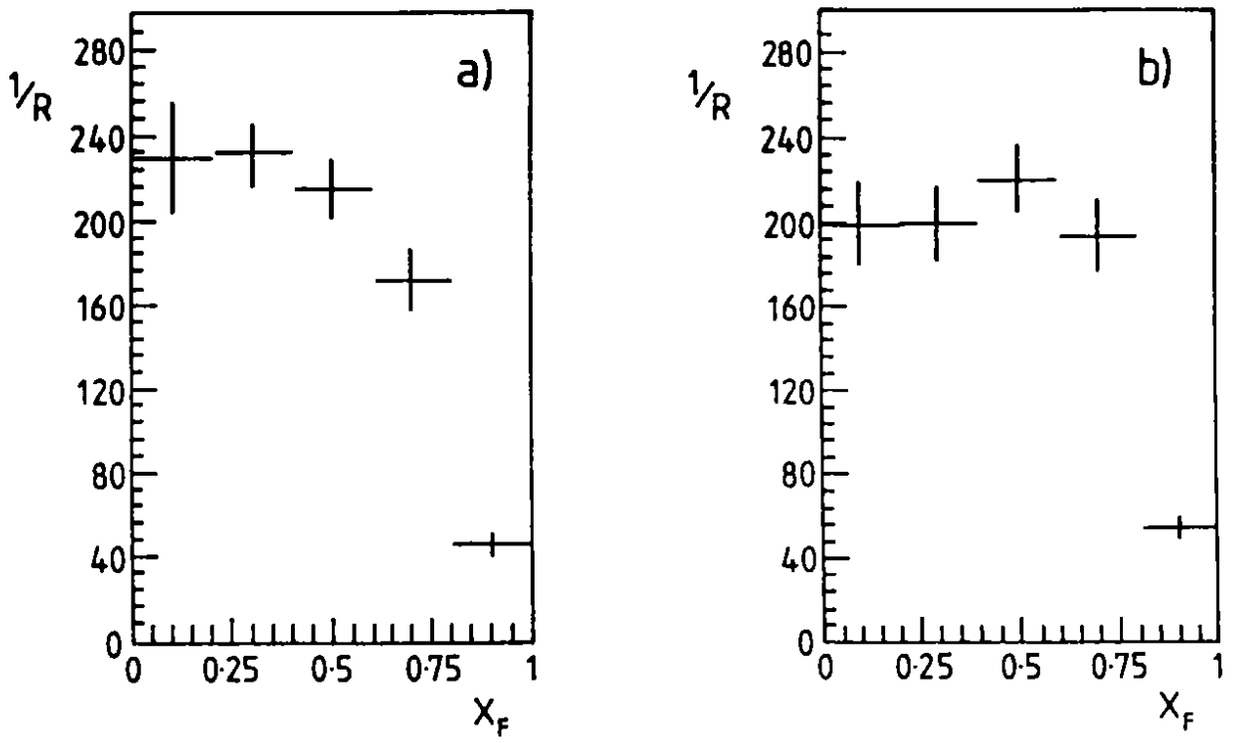

Figure 5: 1/R as a function of x_F for ϕ production at low (a) and high (b) energies.

Further evidence for this change in mechanism in photoproduction at large x_F is provided by study of the decay angular distribution of the ϕ meson in the helicity system. This shows no significant deviation from isotropy at low x_F whereas at high x_F a $\sin^2\theta$ behaviour emerges. A parametrization of this high x_F data has been carried out in complete analogy with [9] in terms of the triple Regge exchange picture with the result shown on figure 6a. The resulting prediction for $d\sigma/dx_F$ is given in figure 6b.

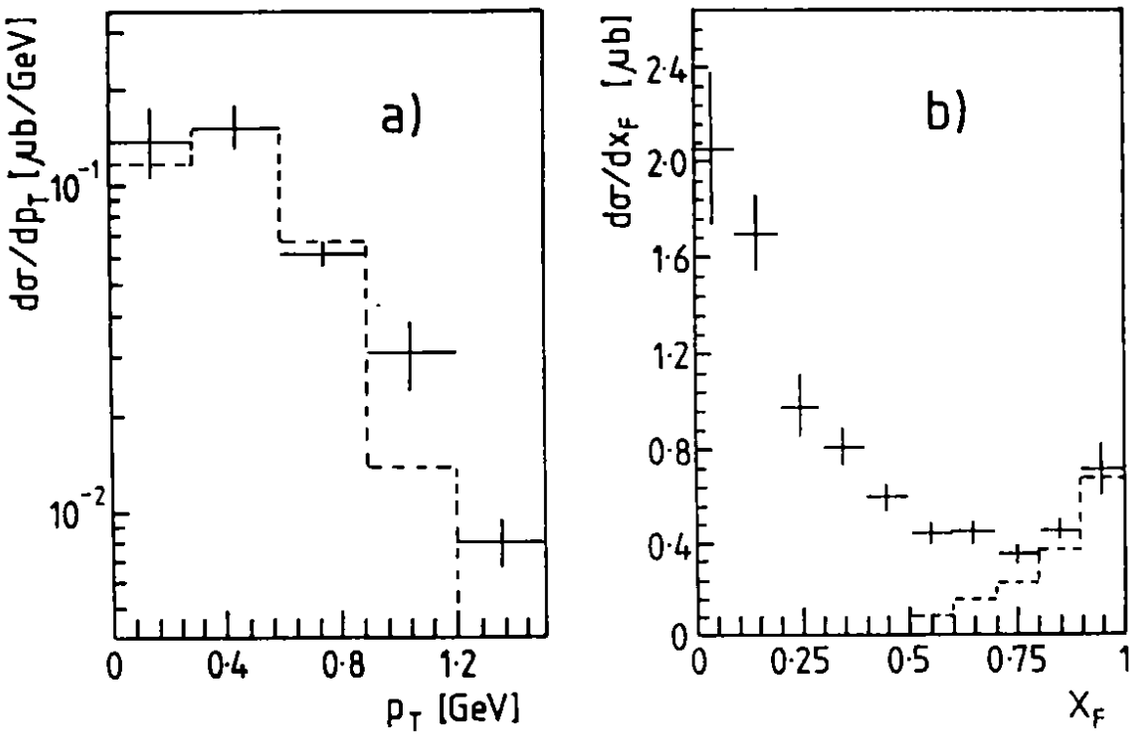

Figure 6: ϕ production in high energy photon data: (a) $d\sigma/dp_T$ for $x_F(\phi) > 0.8$, (b) $d\sigma/dx_F$; the dashed histograms show the triple Regge prediction for quasi diffractive production.

4.2 K^{*0} and $\overline{K^{*0}}$ production.

Tables 4 to 9 show cross sections for $K^{*0}/\ \overline{K^{*0}}$ production. Due to the reflection of the ρ^0 into the $K\pi$ mass distribution, the region $x_F > 0.7$ is excluded from the analysis in the photon and pion induced samples. The contribution to $K^{*0}/\ \overline{K^{*0}}(892)$ production from the decay of higher mass $K^{*0}/\ \overline{K^{*0}}$ mesons is less than 10% [23] and does not affect the analysis discussed in section 5 in any significant way. Again no significant variation with projectile energy is observed and again data are compatible, where comparisons are possible, with previous work.

		$x_F \longrightarrow$						
		0.0-0.1	0.1-0.2	0.2-0.3	0.3-0.4	0.4-0.5	0.5-0.6	0.6-0.7
γ_{low} p_T [GeV/c] ↓	0.0-0.3	–	8.00 ±0.85	4.31 ±0.46	2.47 ±0.23	1.14 ±0.22	1.06 ±0.14	1.10 ±0.13
	0.3-0.6	–	11.68 ±1.42	6.50 ±0.72	3.24 ±0.41	2.68 ±0.22	1.37 ±0.27	1.10 ±0.12
	0.6-0.9	–	7.06 ±0.56	4.50 ±0.48	2.29 ±0.23	2.06 ±0.27	1.06 ±0.24	0.84 ±0.13
	0.9-1.2	–	2.91 ±0.40	1.76 ±0.24	0.93 ±0.09	0.56 ±0.13	0.47 ±0.09	0.22 ±0.06
	1.2-1.5	–	0.69 ±0.26	0.55 ±0.13	0.31 ±0.10	0.34 ±0.10	0.19 ±0.07	0.12 ±0.04
	1.5-1.8	–	0.11 ±0.09	0.35 ±0.06	0.17 ±0.02	0.04 ±0.03	0.03 ±0.02	0.03 ±0.01
γ_{high}	0.0-0.3	11.71 ± 2.01	7.31 ±0.85	4.62 ±0.38	2.53 ±0.29	1.90 ±0.21	1.12 ±0.21	1.02 ±0.18
	0.3-0.6	22.36 ± 5.88	9.47 ±0.72	5.89 ±0.49	4.06 ±0.40	2.86 ±0.31	2.31 ±0.26	0.55 ±0.18
	0.6-0.9	8.94 ± 1.24	4.92 ±0.82	2.83 ±0.70	2.17 ±0.30	2.73 ±0.18	1.00 ±0.16	0.69 ±0.17
	0.9-1.2	2.65 ± 0.76	2.73 ±0.45	0.99 ±0.27	1.40 ±0.25	0.43 ±0.04	0.36 ±0.03	0.65 ±0.05
	1.2-1.5	1.09 ± 0.67	0.85 ±0.22	0.57 ±0.12	0.54 ±0.11	0.39 ±0.10	0.11 ±0.07	0.00 ±0.05
	1.5-1.8	0.33 ± 0.14	0.06 ±0.09	0.17 ±0.06	0.07 ±0.06	0.05 ±0.06	0.10 ±0.03	0.03 ±0.07

Table 4: Differential cross sections $d^2\sigma/(dx_F dp_T)$ (in μb/GeV/c) for photon induced K^{*0} production in the range of $p_T < 1.8$ GeV/c and $0.1 < x_F < 0.7$ for low, and $0.0 < x_F < 0.7$ for high beam energy. The errors listed are purely statistical and an entry 0.00 indicates a statistical error of < 0.005.

		$x_F \longrightarrow$						
		0.0-0.1	0.1-0.2	0.2-0.3	0.3-0.4	0.4-0.5	0.5-0.6	0.6-0.7
π^+_{low} p_T [GeV/c] ↓	0.0-0.3	–	1.09 ± 0.18	0.95 ± 0.11	0.15 ± 0.07	0.06 ± 0.17	0.08 ± 0.02	0.08 ± 0.04
	0.3-0.6	–	1.33 ± 0.27	1.00 ± 0.16	0.30 ± 0.08	0.27 ± 0.08	0.07 ± 0.04	0.13 ± 0.02
	0.6-0.9	–	0.85 ± 0.26	0.43 ± 0.09	0.21 ± 0.07	0.15 ± 0.03	0.05 ± 0.03	0.02 ± 0.02
	0.9-1.2	–	0.21 ± 0.10	0.19 ± 0.07	0.09 ± 0.04	0.05 ± 0.03	0.01 ± 0.01	0.04 ± 0.01
	1.2-1.5	–	0.23 ± 0.05	0.00 ± 0.02	0.02 ± 0.02	0.04 ± 0.01	0.02 ± 0.01	0.00 ± 0.01
	1.5-1.8	–	0.05 ± 0.03	0.04 ± 0.02	0.01 ± 0.02	0.01 ± 0.01	0.01 ± 0.01	-0.01 ± 0.00
π^+_{high}	0.0-0.3	2.33 ± 0.41	1.70 ± 0.18	0.54 ± 0.05	0.24 ± 0.04	0.23 ± 0.07	0.10 ± 0.03	0.18 ± 0.03
	0.3-0.6	3.78 ± 0.49	2.41 ± 0.17	0.99 ± 0.10	0.58 ± 0.05	0.24 ± 0.05	0.22 ± 0.03	0.33 ± 0.05
	0.6-0.9	1.92 ± 0.18	0.93 ± 0.11	0.50 ± 0.08	0.31 ± 0.04	0.19 ± 0.04	0.14 ± 0.03	0.09 ± 0.04
	0.9-1.2	0.49 ± 0.10	0.52 ± 0.09	0.46 ± 0.04	0.18 ± 0.01	0.04 ± 0.02	0.02 ± 0.02	0.06 ± 0.01
	1.2-1.5	0.18 ± 0.05	0.13 ± 0.03	0.07 ± 0.01	0.03 ± 0.09	0.02 ± 0.02	0.03 ± 0.01	0.00 ± 0.02
	1.5-1.8	0.08 ± 0.03	0.06 ± 0.01	0.05 ± 0.01	0.04 ± 0.01	0.01 ± 0.01	0.00 ± 0.01	0.01 ± 0.00
π^-_{low}	0.0-0.3	–	1.71 ± 0.22	1.01 ± 0.15	0.54 ± 0.08	0.31 ± 0.05	0.26 ± 0.03	0.24 ± 0.03
	0.3-0.6	–	1.74 ± 0.32	1.89 ± 0.18	0.87 ± 0.10	0.69 ± 0.06	0.45 ± 0.05	0.43 ± 0.02
	0.6-0.9	–	1.26 ± 0.23	1.12 ± 0.13	0.52 ± 0.09	0.47 ± 0.10	0.36 ± 0.04	0.24 ± 0.02
	0.9-1.2	–	0.92 ± 0.13	0.21 ± 0.08	0.24 ± 0.04	0.16 ± 0.03	0.15 ± 0.02	0.08 ± 0.01
	1.2-1.5	–	0.13 ± 0.04	0.13 ± 0.06	0.11 ± 0.03	0.02 ± 0.02	0.03 ± 0.01	0.02 ± 0.00
	1.5-1.8	–	0.10 ± 0.03	0.08 ± 0.02	0.02 ± 0.01	0.00 ± 0.01	0.00 ± 0.00	0.00 ± 0.00
π^-_{high}	0.0-0.3	1.73 ± 0.30	0.95 ± 0.12	0.66 ± 0.08	0.62 ± 0.06	0.52 ± 0.06	0.24 ± 0.05	0.26 ± 0.05
	0.3-0.6	2.68 ± 0.40	1.66 ± 0.17	1.21 ± 0.10	1.12 ± 0.09	0.60 ± 0.07	0.48 ± 0.05	0.40 ± 0.05
	0.6-0.9	1.64 ± 0.28	0.85 ± 0.12	0.58 ± 0.08	0.76 ± 0.10	0.46 ± 0.05	0.37 ± 0.04	0.37 ± 0.03
	0.9-1.2	0.75 ± 0.03	0.41 ± 0.08	0.17 ± 0.03	0.23 ± 0.04	0.17 ± 0.02	0.08 ± 0.02	0.16 ± 0.02
	1.2-1.5	0.30 ± 0.07	0.19 ± 0.03	0.15 ± 0.03	0.08 ± 0.20	0.04 ± 0.02	0.06 ± 0.01	0.04 ± 0.01
	1.5-1.8	0.14 ± 0.03	0.01 ± 0.02	0.03 ± 0.02	0.05 ± 0.01	0.02 ± 0.01	0.02 ± 0.01	0.00 ± 0.01

Table 5: Differential cross sections $d^2\sigma/(dx_F dp_T)$ (in mb/GeV/c) for pion induced K^{*0} production in the range of $p_T < 1.8$ GeV/c and $0.1 < x_F < 0.7$ for low and $0 < x_F < 0.7$ for high beam energy. The errors listed are purely statistical and an entry 0.00 indicates a statistical error of < 0.005.

		x_F →									
		0.0-0.1	0.1-0.2	0.2-0.3	0.3-0.4	0.4-0.5	0.5-0.6	0.6-0.7	0.7-0.8	0.8-0.9	0.9-1.0
K^+_{low} p_T [GeV/c] ↓	0.0-0.3	–	2.39 ± 0.53	3.05 ± 0.43	1.53 ± 0.18	1.53 ± 0.14	1.07 ± 0.12	1.23 ± 0.09	1.18 ± 0.10	1.13 ± 0.09	0.39 ± 0.12
	0.3-0.6	–	2.07 ± 0.66	3.37 ± 0.55	3.68 ± 0.27	2.32 ± 0.19	2.78 ± 0.20	1.72 ± 0.08	1.39 ± 0.13	1.08 ± 0.09	0.26 ± 0.19
	0.6-0.9	–	3.06 ± 0.44	2.51 ± 0.66	2.00 ± 0.21	1.62 ± 0.15	1.46 ± 0.14	1.33 ± 0.07	0.69 ± 0.06	0.37 ± 0.08	0.15 ± 0.11
	0.9-1.2	–	1.00 ± 0.33	0.89 ± 0.17	0.38 ± 0.14	0.46 ± 0.12	0.51 ± 0.08	0.37 ± 0.05	0.17 ± 0.06	0.08 ± 0.04	–
	1.2-1.5	–	0.21 ± 0.14	0.67 ± 0.07	0.18 ± 0.03	0.23 ± 0.04	0.14 ± 0.04	0.04 ± 0.03	0.03 ± 0.04	0.01 ± 0.01	–
	1.5-1.8	–	0.12 ± 0.05	0.05 ± 0.04	-0.02 ± 0.03	0.04 ± 0.03	0.02 ± 0.16	0.01 ± 0.04	–	–	–
K^+_{high}	0.0-0.3	2.99 ± 0.72	2.46 ± 0.20	2.19 ± 0.05	1.88 ± 0.17	1.69 ± 0.08	1.31 ± 0.06	1.18 ± 0.08	1.37 ± 0.06	1.36 ± 0.06	0.88 ± 0.08
	0.3-0.6	5.84 ± 0.53	4.00 ± 0.18	3.48 ± 0.20	3.15 ± 0.22	2.66 ± 0.16	2.17 ± 0.11	1.99 ± 0.08	1.81 ± 0.11	1.37 ± 0.05	0.65 ± 0.04
	0.6-0.9	2.17 ± 0.41	2.72 ± 0.19	1.81 ± 0.15	2.10 ± 0.18	1.87 ± 0.16	1.61 ± 0.08	1.27 ± 0.09	0.91 ± 0.06	0.52 ± 0.05	0.19 ± 0.02
	0.9-1.2	1.38 ± 0.14	0.96 ± 0.07	0.97 ± 0.14	0.76 ± 0.08	0.87 ± 0.12	0.57 ± 0.05	0.55 ± 0.06	0.32 ± 0.02	0.13 ± 0.03	0.02 ± 0.01
	1.2-1.5	0.34 ± 0.09	0.52 ± 0.11	0.30 ± 0.07	0.33 ± 0.05	0.17 ± 0.04	0.13 ± 0.04	0.21 ± 0.02	0.09 ± 0.04	0.03 ± 0.01	0.00 ± 0.02
	1.5-1.8	0.18 ± 0.05	0.26 ± 0.03	0.15 ± 0.03	0.10 ± 0.03	0.07 ± 0.01	0.03 ± 0.01	0.05 ± 0.17	0.03 ± 0.02	–	–
K^-_{low}	0.0-0.3	–	-0.07 ± 0.58	0.54 ± 0.29	0.10 ± 0.14	0.09 ± 0.09	0.17 ± 0.07	-0.03 ± 0.06	-0.01 ± 0.08	0.05 ± 0.02	–
	0.3-0.6	–	1.11 ± 0.53	0.64 ± 0.37	0.37 ± 0.14	0.06 ± 0.11	0.11 ± 0.07	-0.02 ± 0.07	0.10 ± 0.06	-0.04 ± 0.06	–
	0.6-0.9	–	0.03 ± 0.52	0.53 ± 0.19	0.23 ± 0.12	0.17 ± 0.12	0.11 ± 0.06	0.01 ± 0.05	0.01 ± 0.07	0.01 ± 0.01	–
	0.9-1.2	–	0.55 ± 0.21	0.16 ± 0.10	0.07 ± 0.10	0.06 ± 0.04	0.04 ± 0.01	0.08 ± 0.02	0.07 ± 0.07	-0.04 ± 0.17	–
	1.2-1.5	–	0.04 ± 0.09	0.14 ± 0.09	0.04 ± 0.06	0.00 ± 0.02	–	–	–	–	–
	1.5-1.8	–	-0.02 ± 0.02	0.01 ± 0.02	0.03 ± 0.14	0.05 ± 0.02	–	–	–	–	–
K^-_{high}	0.0-0.3	1.26 ± 0.40	0.74 ± 0.20	0.33 ± 0.13	0.28 ± 0.09	0.13 ± 0.05	0.14 ± 0.05	0.00 ± 0.04	0.01 ± 0.05	0.11 ± 0.03	-0.01 ± 0.01
	0.3-0.6	0.88 ± 0.56	0.89 ± 0.27	0.94 ± 0.16	0.43 ± 0.09	0.49 ± 0.10	0.26 ± 0.11	0.26 ± 0.13	-0.08 ± 0.18	-0.08 ± 0.04	-0.04 ± 0.03
	0.6-0.9	1.36 ± 0.32	1.10 ± 0.11	0.41 ± 0.11	0.29 ± 0.09	0.38 ± 0.08	0.04 ± 0.07	0.13 ± 0.04	0.13 ± 0.07	0.05 ± 0.03	0.00 ± 0.13
	0.9-1.2	1.00 ± 0.20	0.27 ± 0.10	0.06 ± 0.07	0.13 ± 0.05	0.00 ± 0.05	-0.02 ± 0.07	-0.01 ± 0.04	-0.01 ± 0.00	-0.03 ± 0.04	-0.01 ± 0.10
	1.2-1.5	0.36 ± 0.08	0.10 ± 0.04	0.07 ± 0.16	0.01 ± 0.04	0.02 ± 0.02	0.03 ± 0.02	-0.01 ± 0.07	0.02 ± 0.01	0.02 ± 0.02	–
	1.5-1.8	0.13 ± 0.04	-0.03 ± 0.02	0.05 ± 0.03	0.01 ± 0.01	-0.01 ± 0.02	0.01 ± 0.02	0.01 ± 0.01	–	–	–

Table 6: Differential cross sections $d^2\sigma/(dx_F dp_T)$ (in mb/GeV/c) for kaon induced K^{*0} production in the range of $p_T < 1.8$ GeV/c and $0.1 < x_F < 1.0$ for low and $0.0 < x_F < 1.0$ for high beam energy. The errors listed are purely statistical.

		$x_F \longrightarrow$						
		0.0-0.1	0.1-0.2	0.2-0.3	0.3-0.4	0.4-0.5	0.5-0.6	0.6-0.7
γ_{low} p_T [GeV/c] ↓	0.0-0.3	–	4.89 ± 0.70	4.07 ± 0.54	1.95 ± 0.37	1.36 ± 0.19	0.61 ± 0.18	0.79 ± 0.17
	0.3-0.6	–	9.04 ± 0.94	6.00 ± 0.57	3.91 ± 0.41	2.37 ± 0.36	1.19 ± 0.20	1.01 ± 0.15
	0.6-0.9	–	5.89 ± 0.63	3.79 ± 0.39	2.36 ± 0.27	1.59 ± 0.21	0.93 ± 0.14	0.53 ± 0.09
	0.9-1.2	–	2.58 ± 0.30	0.77 ± 0.26	0.73 ± 0.19	0.88 ± 0.13	0.28 ± 0.13	0.15 ± 0.02
	1.2-1.5	–	0.37 ± 0.16	0.50 ± 0.04	0.38 ± 0.11	0.38 ± 0.06	0.13 ± 0.07	0.20 ± 0.03
	1.5-1.8	–	0.20 ± 0.06	0.30 ± 0.11	0.13 ± 0.05	0.05 ± 0.03	0.08 ± 0.03	0.01 ± 0.03
γ_{high}	0.0-0.3	11.07 ±1.27	7.88 ± 0.72	3.72 ± 0.45	2.01 ± 0.41	1.34 ± 0.13	0.79 ± 0.19	0.77 ± 0.18
	0.3-0.6	15.82 ±2.01	9.64 ± 0.69	5.30 ± 0.69	3.13 ± 0.22	2.46 ± 0.39	2.12 ± 0.31	0.98 ± 0.17
	0.6-0.9	8.01 ±1.16	4.49 ± 0.58	3.17 ± 0.36	1.74 ± 0.45	1.83 ± 0.34	1.12 ± 0.17	0.51 ± 0.13
	0.9-1.2	2.17 ±0.56	2.03 ± 0.42	1.18 ± 0.22	0.98 ± 0.16	0.67 ± 0.20	0.14 ± 0.09	0.52 ± 0.09
	1.2-1.5	0.19 ±0.14	0.97 ± 0.29	0.61 ± 0.32	0.58 ± 0.12	0.45 ± 0.10	0.10 ± 0.07	0.00 ± 0.05
	1.5-1.8	0.56 ±0.36	0.23 ± 0.14	0.19 ± 0.07	0.11 ± 0.05	0.05 ± 0.04	0.05 ± 0.04	0.02 ± 0.03

Table 7: Differential cross sections $d^2\sigma/(dx_F dp_T)$ (in μb/GeV/c) for photon induced $\overline{K^{*0}}$ production in the range of $p_T < 1.8$ GeV/c and $0.1 < x_F < 0.7$ for low and $0.0 < x_F < 0.7$ for high beam energy. The errors listed are purely statistical.

5 Discussion of the data in terms of the parton fusion model

5.1 ϕ production

The parton fusion model has been applied to the x_F dependence of the production of ϕ mesons by photon, pion and kaon beams. Data at high x_F, defined as $x_F(\phi) > 0.9$ for photon and kaon beams and $x_F(\phi) > 0.6$ for pion beams, were excluded from this comparison. Zweig-allowed quark fusion, Zweig-suppressed quark fusion, and gluon-gluon fusion (where the intermediate C=+1 state transforms into a ϕ by the emission of a third gluon) are allowed. The contributions of the various processes are shown in Table 10.

The kinematics of the Drell-Yan process fix, for a given x_F, the Bjorken-x of the fusing partons from the target and the beam, and in the kinematical range covered here ($x_F > 0.0$) the Bjorken-x of the partons from the proton is always small (typically 0.006 to 0.06). Figures 7, (a) and (b), show the ratio of ϕ production with π^+/π^- and K^+/K^- beams. Charge conjugation, on the basis of the symmetry of the $s/\bar{s}$ sea, and the absence of strange valence quarks in the proton, predicts that these ratios should be unity provided the Zweig suppressed VV term is small. The data are consistent with unity and show that the non-symmetrical term is negligibly small ($< 5\%$) for both pion and kaon beam data. The ratios for ϕ production by kaon and pion beams are shown in figure 7(c) for K^+/π^+ and in 7(d) for K^-/π^-. These show a rapid rise with increasing x_F from a value close to unity in the central region. The rise can be interpreted by assuming that a strange valence quark from the initial kaon goes over to the ϕ while for the initial pion only sea quarks are available. The value of unity at low x_F suggests that the strange valence quark contribution and the Zweig suppressed VV, VS and V(s)S(s) contributions are all small at low x_F relative to other terms in Table 10.

		$x_F \longrightarrow$						
		0.0-0.1	0.1-0.2	0.2-0.3	0.3-0.4	0.4-0.5	0.5-0.6	0.6-0.7
π^+_{low} p_T [GeV/c] ↓	0.0-0.3	–	1.14 ± 0.18	0.89 ± 0.11	0.68 ± 0.07	0.33 ± 0.04	0.23 ± 0.03	0.20 ± 0.01
	0.3-0.6	–	2.72 ± 0.38	1.18 ± 0.15	0.77 ± 0.07	0.60 ± 0.04	0.48 ± 0.02	0.37 ± 0.02
	0.6-0.9	–	1.67 ± 0.27	0.68 ± 0.08	0.34 ± 0.05	0.28 ± 0.04	0.27 ± 0.04	0.25 ± 0.02
	0.9-1.2	–	0.33 ± 0.11	0.23 ± 0.06	0.25 ± 0.04	0.07 ± 0.02	0.12 ± 0.02	0.12 ± 0.02
	1.2-1.5	–	0.15 ± 0.04	0.14 ± 0.03	0.09 ± 0.02	0.04 ± 0.01	0.03 ± 0.01	0.01 ± 0.01
	1.5-1.8	–	0.06 ± 0.01	0.04 ± 0.01	0.02 ± 0.01	0.02 ± 0.01	0.00 ± 0.01	0.01 ± 0.00
π^+_{high}	0.0-0.3	2.63 ± 0.41	1.28 ± 0.10	0.62 ± 0.07	0.53 ± 0.05	0.48 ± 0.04	0.32 ± 0.03	0.31 ± 0.02
	0.3-0.6	2.97 ± 0.37	1.98 ± 0.16	1.33 ± 0.06	1.08 ± 0.02	0.75 ± 0.05	0.57 ± 0.05	0.48 ± 0.04
	0.6-0.9	2.23 ± 0.22	1.21 ± 0.09	0.71 ± 0.06	0.58 ± 0.06	0.48 ± 0.04	0.38 ± 0.04	0.35 ± 0.05
	0.9-1.2	0.67 ± 0.09	0.45 ± 0.07	0.27 ± 0.04	0.25 ± 0.03	0.19 ± 0.03	0.23 ± 0.02	0.12 ± 0.02
	1.2-1.5	0.20 ± 0.05	0.22 ± 0.03	0.07 ± 0.03	0.07 ± 0.02	0.07 ± 0.06	0.07 ± 0.01	0.04 ± 0.01
	1.5-1.8	0.13 ± 0.03	0.02 ± 0.04	0.06 ± 0.01	0.03 ± 0.01	0.04 ± 0.00	0.02 ± 0.00	0.00 ± 0.00
π^-_{low}	0.0-0.3	–	1.18 ± 0.20	0.59 ± 0.12	0.30 ± 0.07	0.10 ± 0.04	0.13 ± 0.03	0.11 ± 0.03
	0.3-0.6	–	2.05 ± 0.42	0.91 ± 0.17	0.44 ± 0.09	0.07 ± 0.04	0.13 ± 0.01	0.07 ± 0.07
	0.6-0.9	–	0.75 ± 0.23	0.45 ± 0.08	0.09 ± 0.01	0.04 ± 0.03	0.10 ± 0.02	0.05 ± 0.02
	0.9-1.2	–	0.52 ± 0.11	0.10 ± 0.09	0.15 ± 0.03	0.04 ± 0.03	0.02 ± 0.03	0.03 ± 0.01
	1.2-1.5	–	0.13 ± 0.04	0.04 ± 0.03	0.05 ± 0.02	0.00 ± 0.01	0.01 ± 0.01	0.01 ± 0.01
	1.5-1.8	–	0.05 ± 0.02	0.01 ± 0.01	0.01 ± 0.00	0.00 ± 0.00	0.00 ± 0.00	0.00 ± 0.01
π^-_{high}	0.0-0.3	1.91 ± 0.23	0.88 ± 0.15	0.67 ± 0.07	0.40 ± 0.11	0.24 ± 0.05	0.40 ± 0.06	0.16 ± 0.04
	0.3-0.6	2.53 ± 0.33	1.93 ± 0.17	0.86 ± 0.10	0.67 ± 0.09	0.42 ± 0.08	0.23 ± 0.05	0.21 ± 0.10
	0.6-0.9	1.75 ± 0.24	0.78 ± 0.12	0.58 ± 0.07	0.25 ± 0.07	0.30 ± 0.07	0.35 ± 0.12	0.05 ± 0.06
	0.9-1.2	0.70 ± 0.25	0.27 ± 0.06	0.23 ± 0.04	0.19 ± 0.04	0.10 ± 0.06	0.05 ± 0.03	0.04 ± 0.03
	1.2-1.5	0.15 ± 0.05	0.16 ± 0.03	0.05 ± 0.02	0.03 ± 0.03	-0.05 ± 0.08	0.01 ± 0.02	0.01 ± 0.02
	1.5-1.8	0.06 ± 0.02	0.02 ± 0.02	0.04 ± 0.02	0.02 ± 0.01	0.02 ± 0.01	0.00 ± 0.01	0.00 ± 0.01

Table 8: Differential cross sections $d^2\sigma/(dx_F dp_T)$ (in mb/GeV/c) for pion induced $\overline{K^{*0}}$ production in the range of $p_T < 1.8$ GeV/c and $0.1 < x_F < 0.7$ for low and $0.0 < x_F < 0.7$ for high beam energy. The errors listed are purely statistical and an entry 0.00 indicates a statistical error < 0.005.

		$x_F \longrightarrow$									
		0.0-0.1	0.1-0.2	0.2-0.3	0.3-0.4	0.4-0.5	0.5-0.6	0.6-0.7	0.7-0.8	0.8-0.9	0.9-1.0
K^+_{low} p_T [GeV/c] ↓	0.0-0.3	–	1.33 ± 0.31	0.05 ± 0.18	0.20 ± 0.09	0.15 ± 0.04	0.05 ± 0.03	0.02 ± 0.04	-0.01 ± 0.05	0.00 ± 0.05	0.02 ± 0.01
	0.3-0.6	–	1.13 ± 0.43	0.16 ± 0.14	0.24 ± 0.10	0.06 ± 0.07	-0.01 ± 0.08	0.01 ± 0.05	0.02 ± 0.05	0.03 ± 0.04	0.00 ± 0.00
	0.6-0.9	–	0.21 ± 0.30	0.24 ± 0.17	0.12 ± 0.02	-0.08 ± 0.05	-0.08 ± 0.07	0.03 ± 0.04	-0.04 ± 0.05	-0.01 ± 0.05	–
	0.9-1.2	–	0.15 ± 0.14	-0.11 ± 0.08	0.12 ± 0.07	0.05 ± 0.04	0.01 ± 0.04	-0.01 ± 0.05	-0.02 ± 0.07	–	–
	1.2-1.5	–	0.10 ± 0.07	0.00 ± 0.07	0.03 ± 0.04	0.01 ± 0.05	0.02 ± 0.04	–	–	–	–
	1.5-1.8	–	-0.01 ± 0.06	-0.03 ± 0.04	0.03 ± 0.04	-0.02 ± 0.01	–	–	–	–	–
K^+_{high}	0.0-0.3	2.05 ± 0.39	1.02 ± 0.16	0.06 ± 0.09	-0.04 ± 0.07	0.08 ± 0.04	0.06 ± 0.05	0.04 ± 0.05	0.05 ± 0.03	0.05 ± 0.02	0.02 ± 0.02
	0.3-0.6	2.99 ± 1.00	0.92 ± 0.19	0.52 ± 0.13	0.47 ± 0.10	0.18 ± 0.07	0.17 ± 0.04	0.10 ± 0.04	0.03 ± 0.01	0.00 ± 0.02	0.05 ± 0.05
	0.6-0.9	1.15 ± 0.22	0.82 ± 0.15	0.51 ± 0.09	0.29 ± 0.09	0.07 ± 0.04	0.12 ± 0.06	0.06 ± 0.02	-0.01 ± 0.01	0.02 ± 0.00	0.01 ± 0.02
	0.9-1.2	0.49 ± 0.12	0.11 ± 0.05	0.14 ± 0.04	0.14 ± 0.03	0.06 ± 0.03	0.02 ± 0.01	0.04 ± 0.02	0.04 ± 0.02	0.01 ± 0.01	0.00 ± 0.00
	1.2-1.5	0.01 ± 0.06	-0.04 ± 0.03	0.10 ± 0.02	0.09 ± 0.02	-0.01 ± 0.02	0.00 ± 0.02	-0.01 ± 0.01	0.01 ± 0.01	0.00 ± 0.00	–
	1.5-1.8	0.04 ± 0.03	0.02 ± 0.02	0.02 ± 0.02	-0.01 ± 0.01	0.00 ± 0.00	0.01 ± 0.01	0.00 ± 0.02	0.00 ± 0.03	–	–
K^-_{low}	0.0-0.3	–	1.92 ± 0.28	2.47 ± 0.29	1.82 ± 0.34	1.41 ± 0.18	1.35 ± 0.12	1.05 ± 0.12	0.89 ± 0.10	0.82 ± 0.10	0.19 ± 0.07
	0.3-0.6	–	5.69 ± 0.80	3.80 ± 0.51	2.69 ± 0.34	2.42 ± 0.24	2.39 ± 0.22	1.87 ± 0.13	1.53 ± 0.15	0.84 ± 0.09	0.12 ± 0.07
	0.6-0.9	–	3.50 ± 0.58	2.01 ± 0.47	1.78 ± 0.26	1.66 ± 0.19	1.51 ± 0.55	1.15 ± 0.10	0.86 ± 0.13	0.53 ± 0.09	0.03 ± 0.09
	0.9-1.2	–	1.22 ± 0.27	0.52 ± 0.21	0.68 ± 0.17	0.56 ± 0.12	0.41 ± 0.08	0.37 ± 0.04	0.17 ± 0.06	0.12 ± 0.06	–
	1.2-1.5	–	0.22 ± 0.14	0.25 ± 0.08	0.23 ± 0.06	0.14 ± 0.06	0.09 ± 0.04	0.11 ± 0.05	0.06 ± 0.05	–	–
	1.5-1.8	–	0.04 ± 0.07	0.07 ± 0.05	0.08 ± 0.05	0.01 ± 0.04	-0.02 ± 0.07	-0.01 ± 0.05	–	–	–
K^-_{high}	0.0-0.3	3.75 ± 0.61	2.28 ± 0.24	1.78 ± 0.29	1.78 ± 0.13	1.54 ± 0.05	1.18 ± 0.13	1.10 ± 0.08	1.28 ± 0.07	1.35 ± 0.08	0.69 ± 0.08
	0.3-0.6	4.65 ± 0.51	3.77 ± 0.31	3.57 ± 0.22	2.76 ± 0.23	2.84 ± 0.16	2.00 ± 0.13	1.72 ± 0.11	1.37 ± 0.21	1.04 ± 0.06	0.32 ± 0.05
	0.6-0.9	2.66 ± 0.38	2.70 ± 0.22	1.86 ± 0.27	2.00 ± 0.18	1.77 ± 0.21	1.28 ± 0.11	1.28 ± 0.08	0.74 ± 0.11	0.48 ± 0.04	0.15 ± 0.03
	0.9-1.2	0.42 ± 0.22	0.58 ± 0.17	1.00 ± 0.12	0.59 ± 0.03	0.41 ± 0.11	0.42 ± 0.06	0.36 ± 0.04	0.39 ± 0.05	0.17 ± 0.03	0.05 ± 0.05
	1.2-1.5	0.43 ± 0.10	0.41 ± 0.08	0.21 ± 0.07	0.17 ± 0.04	0.35 ± 0.04	0.09 ± 0.03	0.10 ± 0.04	0.09 ± 0.03	0.00 ± 0.02	0.01 ± 0.04
	1.5-1.8	0.16 ± 0.05	-0.03 ± 0.03	0.05 ± 0.02	0.04 ± 0.02	0.03 ± 0.03	0.02 ± 0.02	0.01 ± 0.02	0.00 ± 0.01	–	–

Table 9: Differential cross sections $d^2\sigma/(dx_F dp_T)$ (in mb/GeV/c) for kaon induced $\overline{K^{*0}}$ production in the range of $p_T < 1.8$ GeV/c and $0.1 < x_F < 1.0$ for low and $0.0 < x_F < 1.0$ for high beam energy. The errors listed are purely statistical and an entry 0.00 indicates a statistical error < 0.005.

	Zweig-allowed		Zweig-suppressed						gluon
beam	V(s)S(s)	S(s)S(s)	VV	VS	V(s)S(s)	SV	SS	S(s)S(s)	GG
ϕ	2	2λ			2	3	4	2λ	1
ρ,ω		2λ	3/2	2		3	4	2λ	1
π^+		2λ	1	2		3	4	2λ	1
π^-		2λ	2	2		3	4	2λ	1
K^+	1	2λ		1	1	3	4	2λ	1
K^-	1	2λ	2	1	1	3	4	2λ	1

Table 10: The relative weight of the different contributions for ϕ production by parton fusion. The notation is that the first of the pair (e.g. V(s) of V(s)S(s)) refers to the projectile and the second (S(s) in this example) refers to the target proton.

Previous workers (see for example [25], [26], [5], [27], and [22]) have fitted their K^{*0} or ϕ meson data to quark fusion models and all conclude that there is plenty of flexibility to provide good fits. A similar procedure here gives the histograms shown on figure 8. Varying the constraints again shows that the quark fusion model has no problem in fitting the data - for more details see [23]. The details of the fit parameters are affected by the uncertainties in the shape of the strange sea of the proton at low x_B and by the range of reasonable assumptions which give acceptable fits. The philosophy of this work has been to concentrate on physically meaningful quantities that are directly deduced from the data. Overall fits were less useful because of the strong correlations between assumptions and the values of fitted parameters. Figure 8 (c) is dominated (except at low x_F) by the strange valence quark of the kaon, which can be parametrised by $x_B^{\alpha}(1-x_B)^{\beta}$, combining with a strange quark from the proton sea. It shows a relatively hard structure function for the strange quark in the kaon. The uncertainty in the strange sea of the proton and to a lesser extent in the contribution from the S(s) S(s) term are largely at low x_F and so reflect into a large uncertainty (at least ± 0.3) in α. However β is less sensitive to these effects and is found to be 0.5 ± 0.1 compared to typically 0.95 for the non-strange quark in the pion: see for example [25].

5.2 K^{*0} and $\overline{K^{*0}}$ production

K^{*0} and $\overline{K^{*0}}$ production has the prospect of stronger constraints on the parton fusion model with exclusively Zweig-allowed diagrams (and so a single coupling constant) and additional information due to the asymmetries associated with the different charge states. On the other hand there are contributions to the cross sections, particularly at high x_F, due to additional mechanisms such as pion exchange, so the range of $x_F(K^{*0}) > 0.8$ for the kaon beams is excluded.

Figures 9 (a), (b) and (c) show the ratios for each of photon, pion and kaon beams for the cases where there is a common quark between the projectile and the final $K^{*0}/\overline{K^{*0}}$. All figures are similar and show ratios close to unity. Deviations from unity would be expected because the number of contributing diagrams is larger for K^{*0} than $\overline{K^{*0}}$ production as only the former allows contributions from a valence quark from the proton (see Table 11). The absence of any significant deviations from unity suggests that the contribution from the valence quarks in the proton is small at the x values probed by this experiment. Similar results have been obtained previously. For example [6] found that K^+ to K^{*0} and K^{*+} at 250 GeV had similar cross sections.

The far greater effect of a common s quark, as opposed to a u/d quark, between the beam

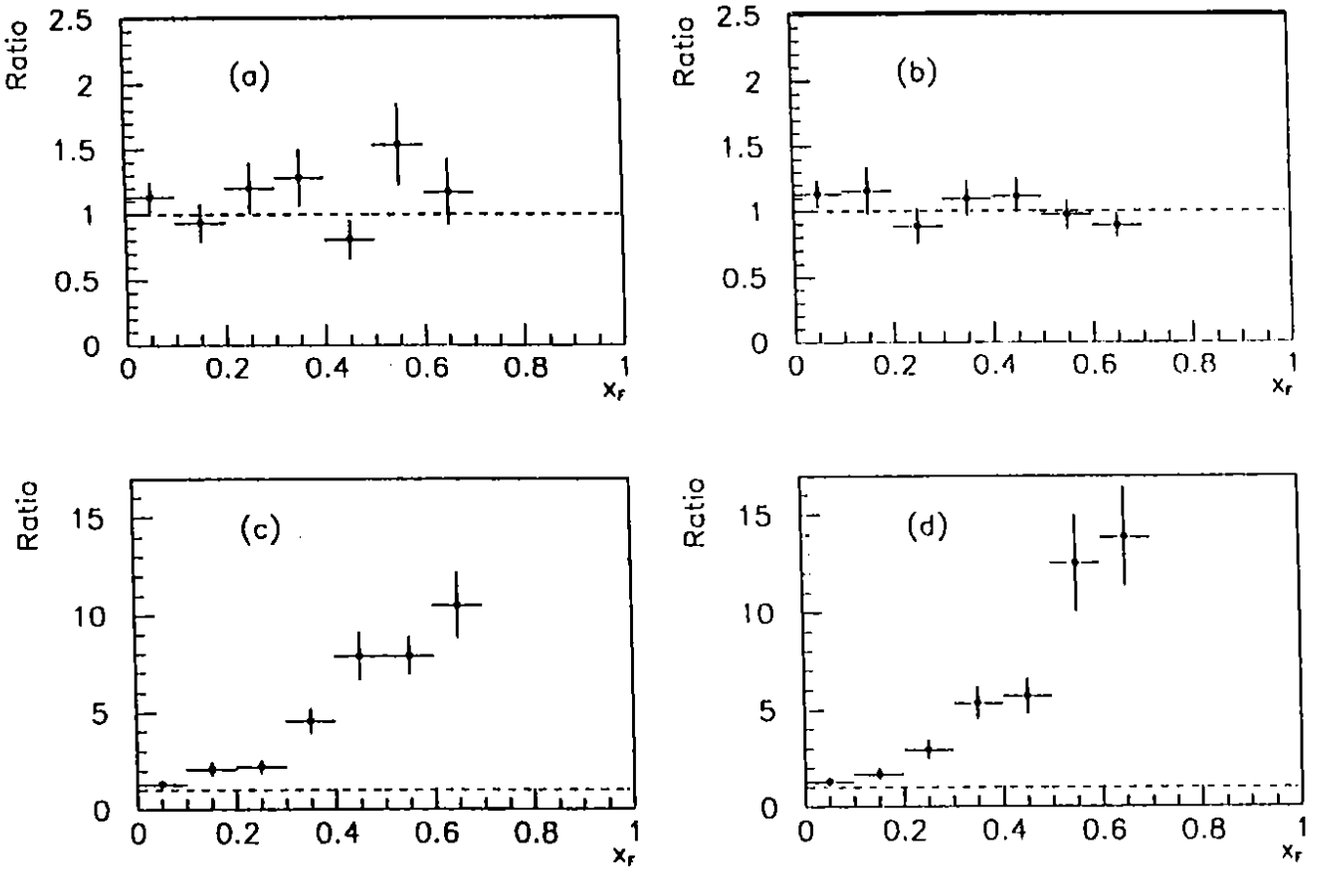

Figure 7: Ratios of ϕ production vs x_F: (a) π^+/π^-, (b) K^+/K^-, (c) K^+/π^+, and (d) K^-/π^- The invariant cross sections are consistent between low and high energies and so ratios of averages are shown.

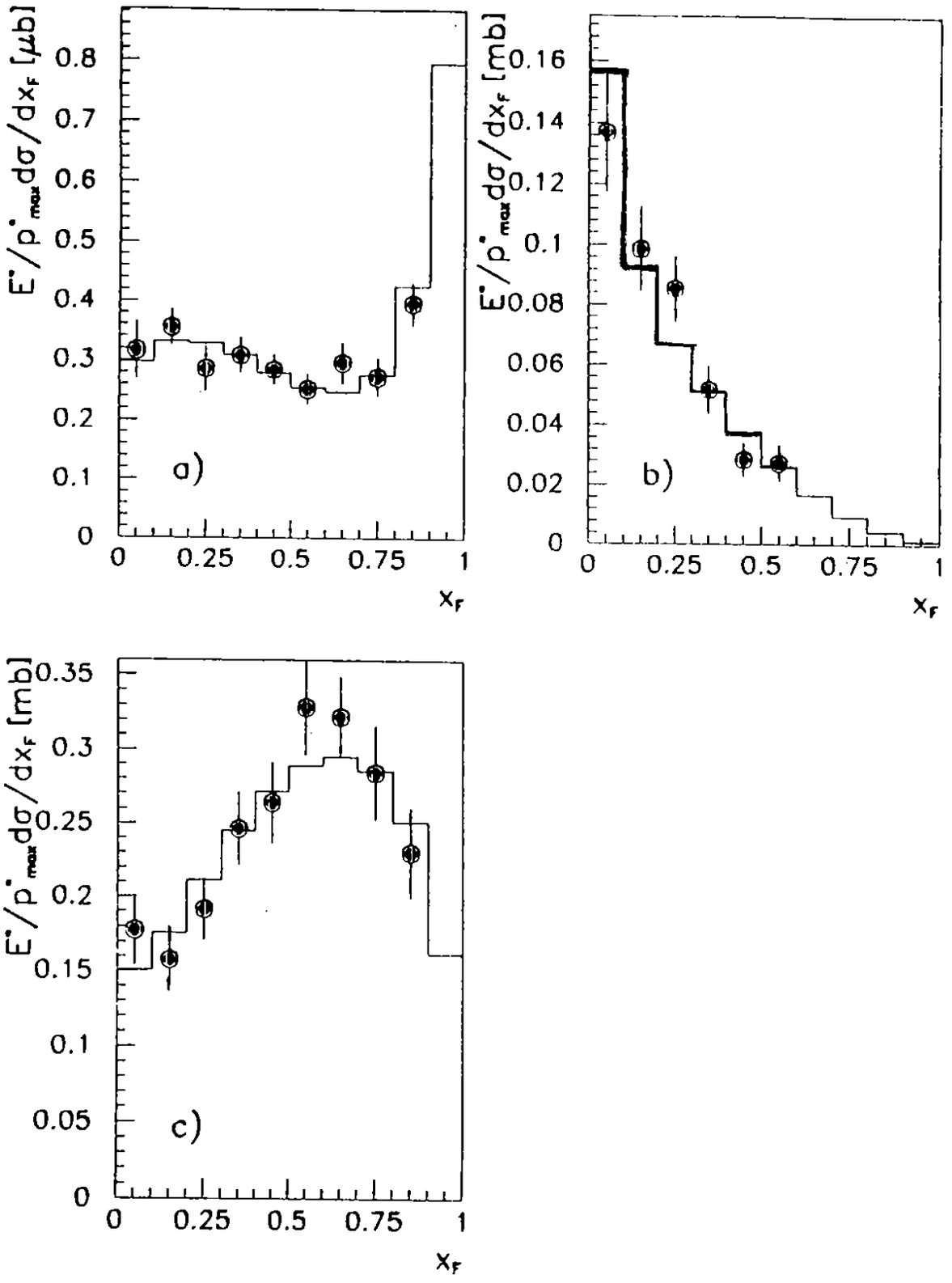

Figure 8: Invariant cross sections for ϕ production as function of x_F compared with predictions of the parton fusion model: (a) photon induced, (b) pion induced, (c) kaon induced data (all high energy); the full line corresponds to a typical fit of the parton fusion model except that (a) shows the sum of the parton fusion and diffractive contributions.

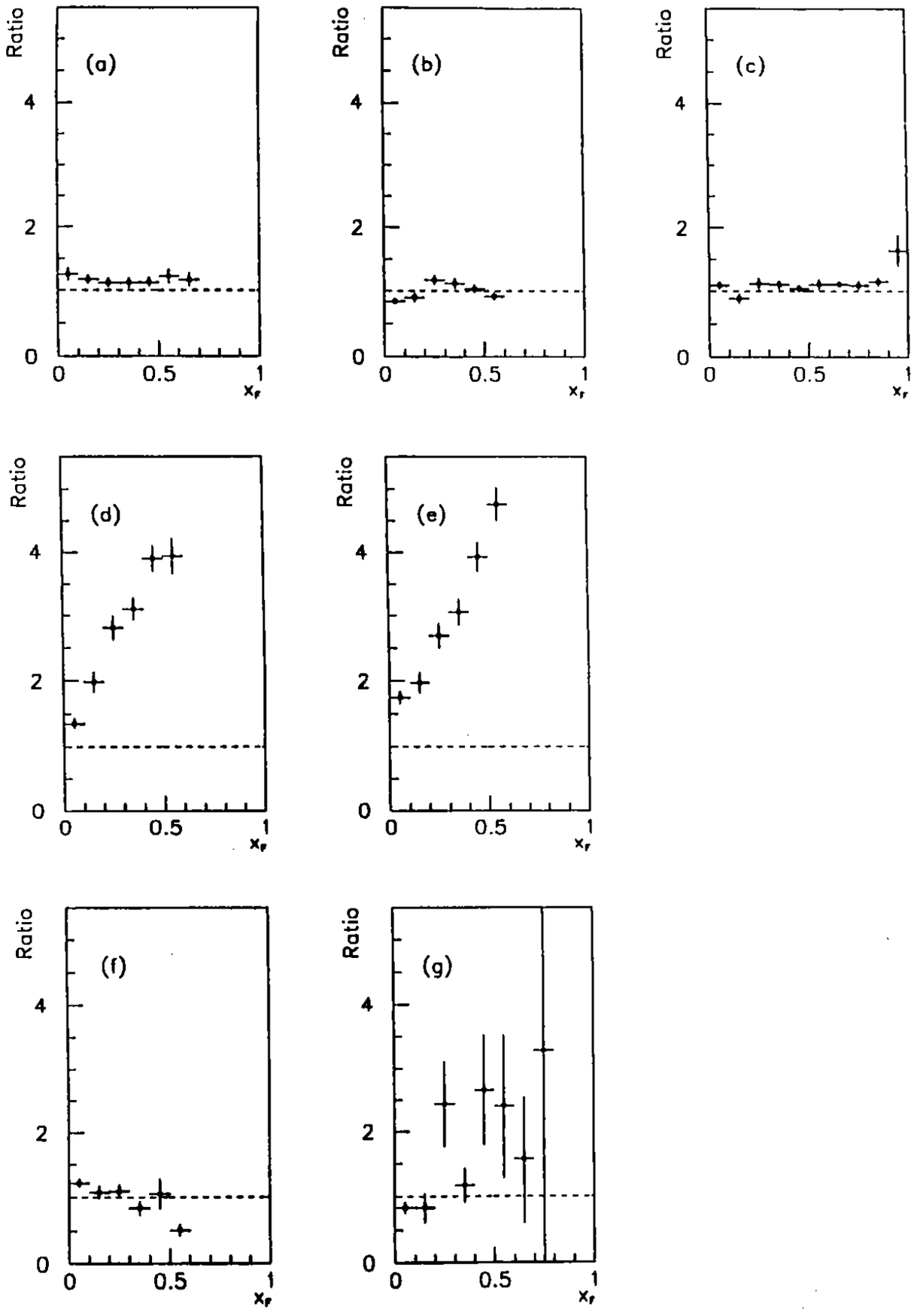

Figure 9: Ratios of cross sections for (a) $\sigma(\gamma \to K^{*0})/\sigma(\gamma \to \overline{K^{*0}})$ (b) $\sigma(\pi^- \to K^{*0})/\sigma(\pi^+ \to \overline{K^{*0}})$ (c) $\sigma(K^+ \to K^{*0})/\sigma(K^- \to \overline{K^{*0}})$ (d) $\sigma(K^- \to \overline{K^{*0}})/\sigma(\pi^+ \to \overline{K^{*0}})$ (e) $\sigma(K^+ \to K^{*0})/\sigma(\pi^- \to K^{*0})$ (f) $\sigma(\pi^+ \to K^{*0})/\sigma(\pi^- \to \overline{K^{*0}})$ (g) $\sigma(K^- \to K^{*0})/\sigma(K^+ \to \overline{K^{*0}})$. The ratios are shown as functions of x_F. The invariant cross sections are consistent between low and high energies and so ratios of averages are shown.

	K^{*0}						$\overline{K^{*0}}$			
beam	V(s)V	VS(s)	V(s)S	S(s)V	S(s)S	SS(s)	V S(s)	V(s)S	S(s)S	SS(s)
ϕ	1		1	λ	λ	1		1	λ	1
ρ,ω		1/2		λ	λ	1	1/2		λ	1
π^+				λ	λ	1	1		λ	1
π^-		1		λ	λ	1			λ	1
K^+	1		1	λ	λ	1			λ	1
K^-				λ	λ	1		1	λ	1

Table 11: Relative weight of the different contributions for $K^{*0}/\overline{K^{*0}}$ production by parton fusion. The notation is the same as that used in Table 10.

particle and the $K^{*0}/\overline{K^{*0}}$ is shown by the rapid rise, to values of order 4, for the ratio of kaon over pion induced reactions (in each case with a common quark) shown in figures 9(d) and (e).

The ratios of cross sections for channels with no common quarks are shown in figures 9 (f) and (g). Here the strange quark must come from the sea while the non-strange quark can come either from the sea or the valence quarks of the proton. Experimentally the much smaller amount of $K^{*0}/\overline{K^{*0}}$ makes extraction of the signal more difficult and thus increases the systematic experimental errors. The S(s)V term would be expected to push the ratio above unity particularly at lower x_F in both figures 9 (f) and (g). There is no evidence here of such an effect and the data tend to support the hypothesis that the proton valence contribution is small.

The invariant cross sections for high energy are shown on figure 10. Here data for $K^{*0}/\overline{K^{*0}}$ has been averaged for each beam. Separate averages are given for cases with/without a common quark between initial and final states. The continuous histogram on the figure is the result of a global fit to the data from all beams carried out in the same way as for the ϕ. It is again successful and shows a hard valence strange quark structure function in the kaon, similar to that given by ϕ production discussed above. The similarity between figure 10 (e) and figure 11 (f) (see below) shows the dominance of the V(s) S contribution to invariant cross sections for channels with a common strange quark. Details of the fit procedure are given in [23] although, there, slightly different input parameters were used.

Table 11 shows how differences in invariant cross sections between different charges of the projectiles measure specific contributions from the parton fusion model. Figure 11 shows the individual invariant cross sections as functions of x_F. The different energies show good agreement and are averaged. In the two separate cases where a given quantity is measured by two different combinations (i.e. figures 11(a) and (b)) they agree well and each of these two plots shows the mean of the two measurements.

Figure 11(b) shows VS(s) for pions, which is given both by $(\pi^- \to K^{*0}) - (\pi^+ \to K^{*0})$ and by $(\pi^+ \to \overline{K^{*0}}) - (\pi^- \to \overline{K^{*0}})$. The average shown is insensitive to the relative normalisation for the different beam charges and the relative acceptance for K^{*0} and $\overline{K^{*0}}$. The result is non-zero and relatively slowly varying with x_F. Figures 11(d) and (f) show the two leading contributions where an $s/\bar{s}$ quark from the incident kaon is transferred to the $K^{*0}/\overline{K^{*0}}$. Figure 11 (d) is determined from $(K^+ \to K^{*0}) + (K^+ \to \overline{K^{*0}}) - (K^- \to K^{*0}) - (K^- \to \overline{K^{*0}})$ and so involves subtracting two large terms. It is the only plot on figure 11 which is significantly sensitive to the relative normalisation for the different beam charges and the systematic errors, not shown on the figure, are typically 0.1 mb in this case. The data show that V(s)V is small and consistent with zero. V(s)S, which comes from $(K^- \to \overline{K^{*0}}) - (K^+ \to \overline{K^{*0}})$, is dominated by the first term and is not sensitive to the relative normalisation. This is much the largest of

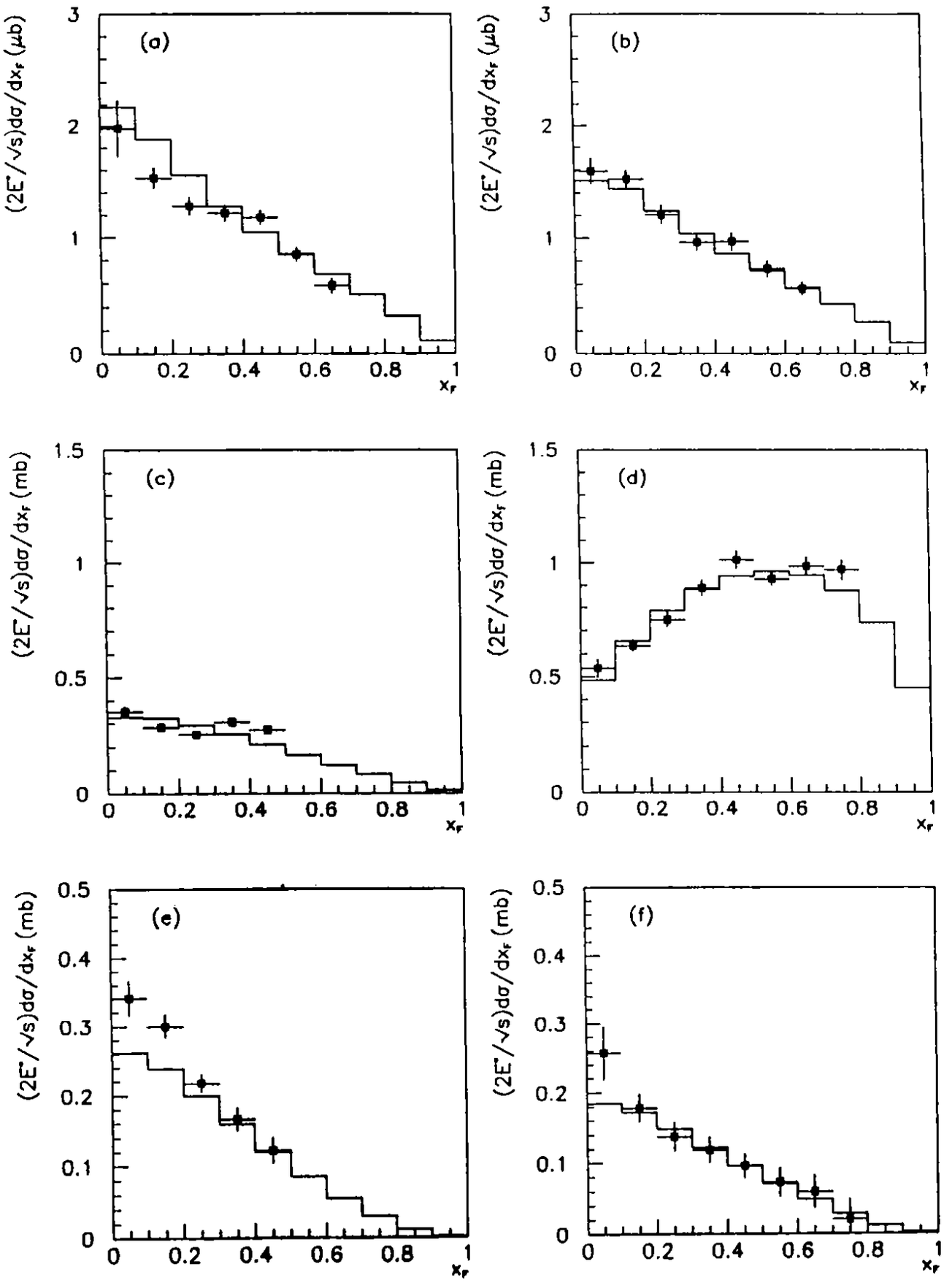

Figure 10: Invariant cross section for $K^{*0}/\overline{K^{*0}}$ production (high energy). (a) photon induced K^{*0}, (b) photon induced $\overline{K^{*0}}$, (c) pion induced with a common quark between the beam and final $K^{*0}/\overline{K^{*0}}$, (d) kaon induced with a common (strange) quark (e) pion induced with no common quark, and (f) kaon induced with no common quark. A parton fusion model global fit is shown as the solid histogram.

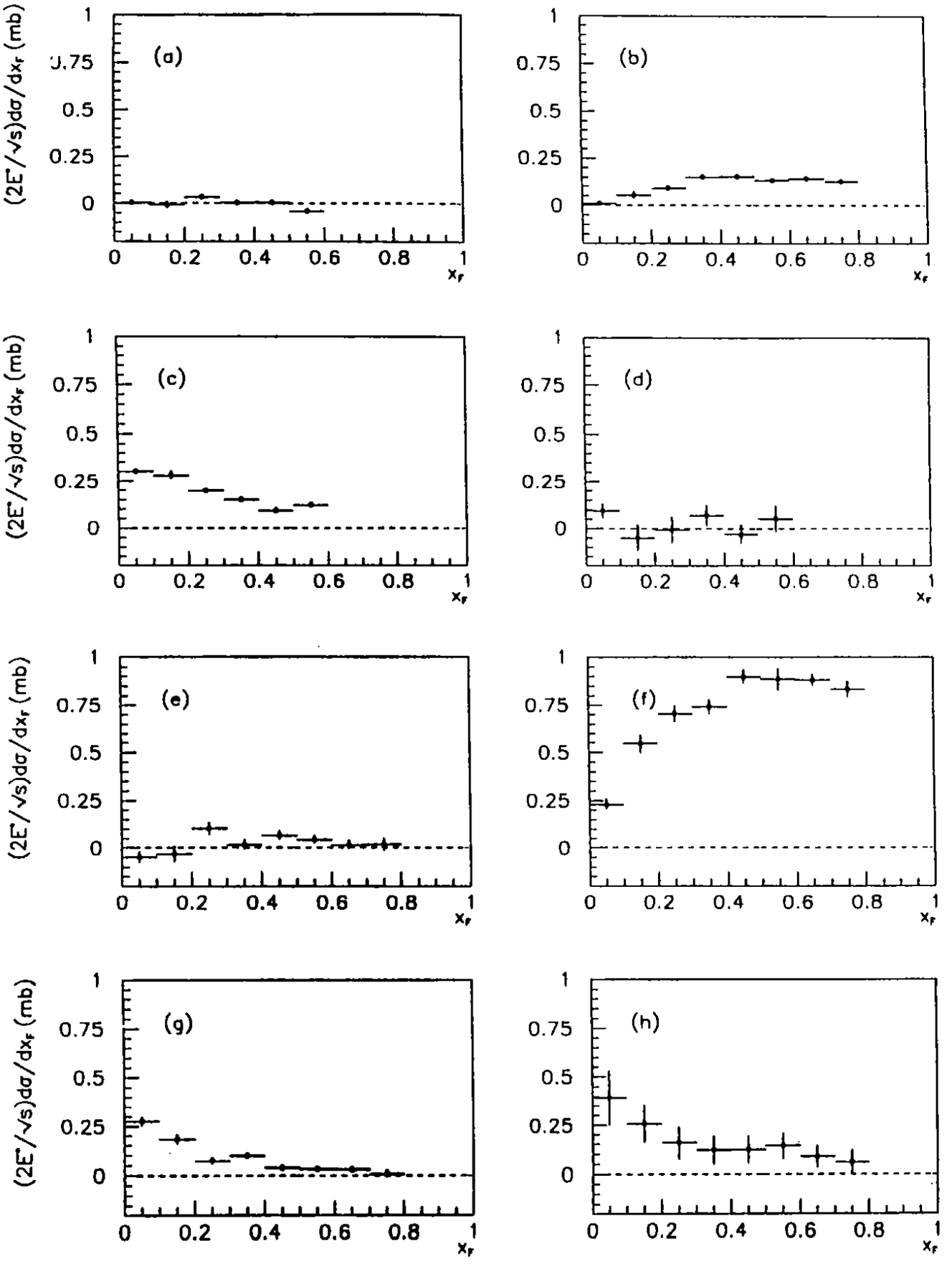

Figure 11: Variations of parton fusion contributions with x_F. (a) λS(s)V for the pion, (b) VS(s) for the pion, (c) λS(s)S + SS(s) for the pion, (d) V(s)V for the kaon (note additional systematic errors - see text), (e) λS(s) V, for the kaon, (f) V(s)S for the kaon, (g) λS(s)S + SS(s) for the kaon, and (h) V(s)V + λS(s)V for the ϕ component and λS(s)V from the ρ/ω component of the γ (the cross section scale must be divided by 1000 for this plot).

all the terms and shows directly the hard nature of the strange quark in the kaon. The small size of V(s)V relative to V(s)S shows that the valence relative to the sea contribution from the proton is small.

It is not possible to separate the λS(s)S and SS(s) components; however their sum is shown to be small but finite for pion and kaon beams in figures 11(c) and (g) respectively. The two are reasonably compatible, indicating that the seas of the pion and kaon are similar.

Figures 11(a) and (e) show that λS(s)V for pions and kaons are both small. This is presumably due both to the relatively small amount of strange sea quark in either the pion or the kaon in the x_F range studied and to the small proton valence contribution. λS(s)V for the pion (figure 11(a)) is given by $(\pi^+ \rightarrow K^{*0}) - (\pi^- \rightarrow \overline{K^{*0}})$ and by $(\pi^- \rightarrow K^{*0}) - (\pi^+ \rightarrow \overline{K^{*0}})$ and the average shown is very insensitive to the relative normalisation for the different beam charges.

Figure 11(h) gives the difference between invariant cross sections for K^{*0} and $\overline{K^{*0}}$ photoproduction. All contributions (see table 11) contain the proton valence term, and so the figure suggests that this term, although small, is finite.

Figure 12(a) shows the average of the π^+ and π^- induced K^{*0} and $\overline{K^{*0}}$ production reactions divided by the average of photoproduction of K^{*0} and $\overline{K^{*0}}$. The strange and non-strange components of the photon must, since each of the ρ^0 ω and ϕ are made up of pairs of quarks of like flavour, have structure functions that are not too dissimilar. For the ρ^0 and ω parts of the photon, table 11 shows that all terms that contribute do so with the same coefficients as the average of π^+ and π^- induced production. The terms originating from the ϕ part of the photon are also rather similar. Thus overall the ratio would be expected to be rather flat with a typical VMD factor of about 200 which is in accord with the data. The corresponding K production of K^{*0} ($\overline{K^{*0}}$) divided by photoproduction (figure 12b) shows a very different behaviour with a steep rise due to the very hard strange quark in the kaon discussed above.

Ratios of the contributions shown on figure 11 enable comparisons of structure functions to be made. The ratio of V(s)V to V(s)S (for kaon data) (figure 13(a)) shows that the non-strange proton valence contribution is much less than the non-strange sea contribution over the whole of the x_B range (typically 0.006 to 0.06). The exact limit depends on systematic effects and is about 15%. Support for a small valence contribution comes from the ratio of λS(s)V to λS(s)S + SS(s) for pions (figure 13(b)). This ratio has small systematic errors. The corresponding ratio for kaons (figure 13(c)) has errors which are too large to allow a significant test. Many current theoretical analyses (e.g. [28], [29], [30]) suggest that valence and sea contributions would be of similar magnitude except at very high Q^2 values although previous experiments support the present conclusion (see for example [10] and [6]).

The results on the nature of the proton structure function suggest that that the presently available structure functions may be inappropriate at the low values of Q^2 probed by this experiment. The $s\bar{s}$ nature of the ϕ excludes the possibility of a corresponding check from ϕ-production channels. Thus the effect observed here would not have been seen in experiments where fewer reactions have been studied.

The ratio of VS(s) for pions to V(s)S for kaons, figure 13 (d), is the product of the ratios of strange to non-strange sea structure functions of the proton and the non-strange valence of the pion to the strange valence of the kaon. If the pairs of sea/valence structure functions have similar x dependences, a constant ratio (as observed) is expected. However the usual assumption is that the strange sea for the proton is about half of the non-strange sea, so if the momentum fraction of the strange quark in the kaon were similar to that of the d quark in the pion, the ratio shown on figure 13 (d) would be expected to be of order 0.5. The ratio of 0.15 shown on the figure again indicates the relative hardness of the strange valence structure

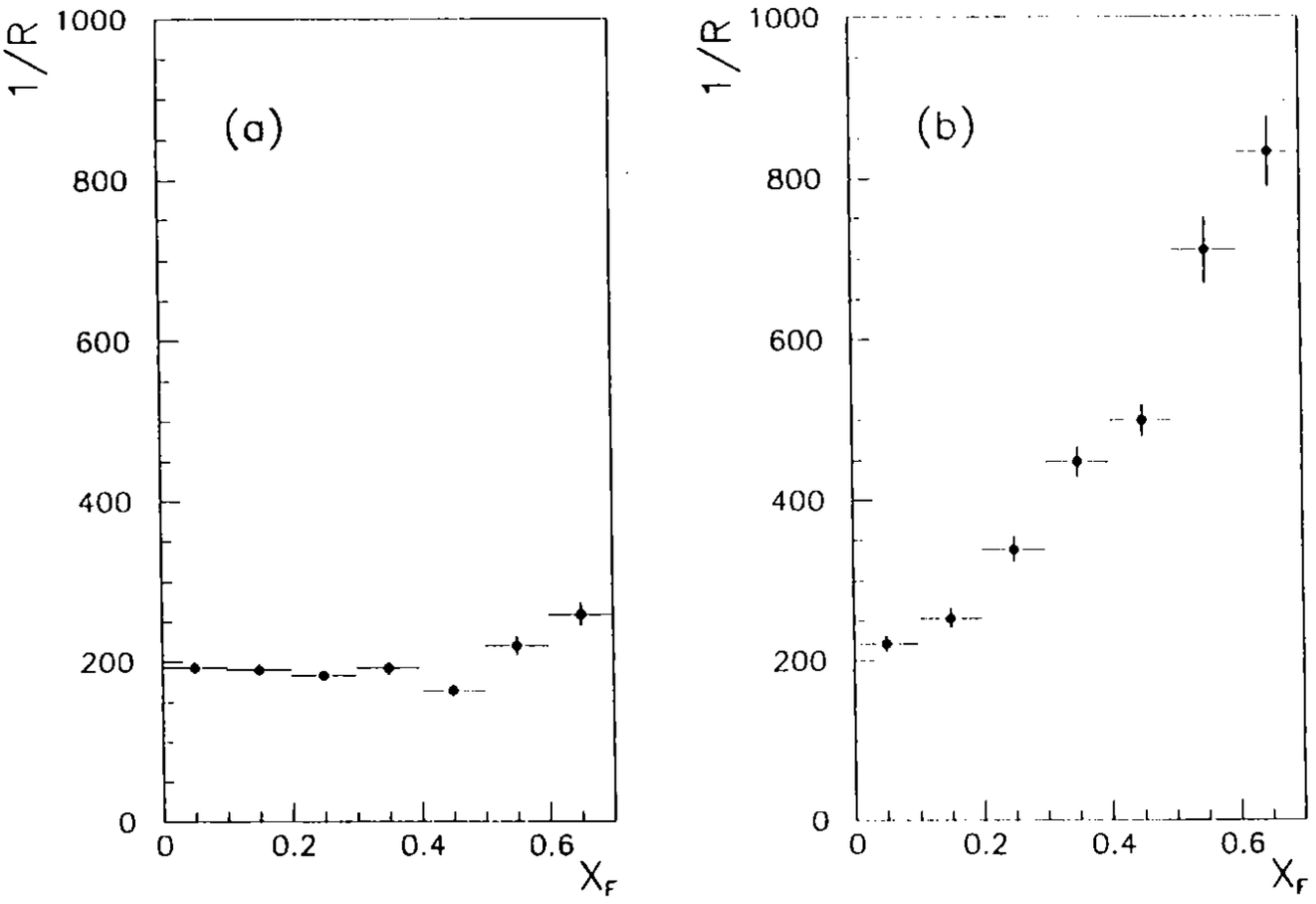

Figure 12: $K^{*0}/\overline{K^{*0}}$ production ratios for (a) pion beam data / photon beam data, (b) kaon beam data / photon beam data.

function of the kaon, with the strange quark carrying most of the kaon momentum. Recently [31] have suggested that, at least at higher Q^2, the strange sea of the proton may be larger than 0.5, which would lead to an even harder strange valence structure function for the kaon.

6 Summary and conclusions

This paper reports on production of ϕ, K^{*0} and $\overline{K^{*0}}$ mesons with photon and hadron beams as a function of x_F and p_T in the energy range from 65 to 175 GeV. An identical detector setup, trigger and software was used for all data. Accounting for experimental resolution effects, ϕ and $K^{*0}/\overline{K^{*0}}$ mass and width parameters were found to be consistent with their nominal values. Comparing photon and hadron data for ϕ production shows good agreement with the vector meson dominance expectations in the range of low x_F. Excluding large x_F phenomena the parton fusion model is shown to give a good description of many parts of the ϕ, K^{*0} and $\overline{K^{*0}}$ production. However the more stringent tests in K^{*0} and $\overline{K^{*0}}$ production show that, within the terms of the model, the contribution of the valence as opposed to the sea quarks from the proton is small and thus quite different from the expectations of a smooth extrapolation to low Q^2 of existing structure function parametrisations. Both ϕ and $K^{*0}/\overline{K^{*0}}$ production show that the strange valence structure function in the kaon is hard.

Acknowledgements
The financial help of BMFT-Foerderkennzeichen 05-4BN14P(0) (Germany) and SERC (U.K.) is gratefully acknowledged. Many technicians and the CERN OMEGA and beam line groups made vital contributions to the work. The computer centres at Bonn (RHRZ), RAL, and

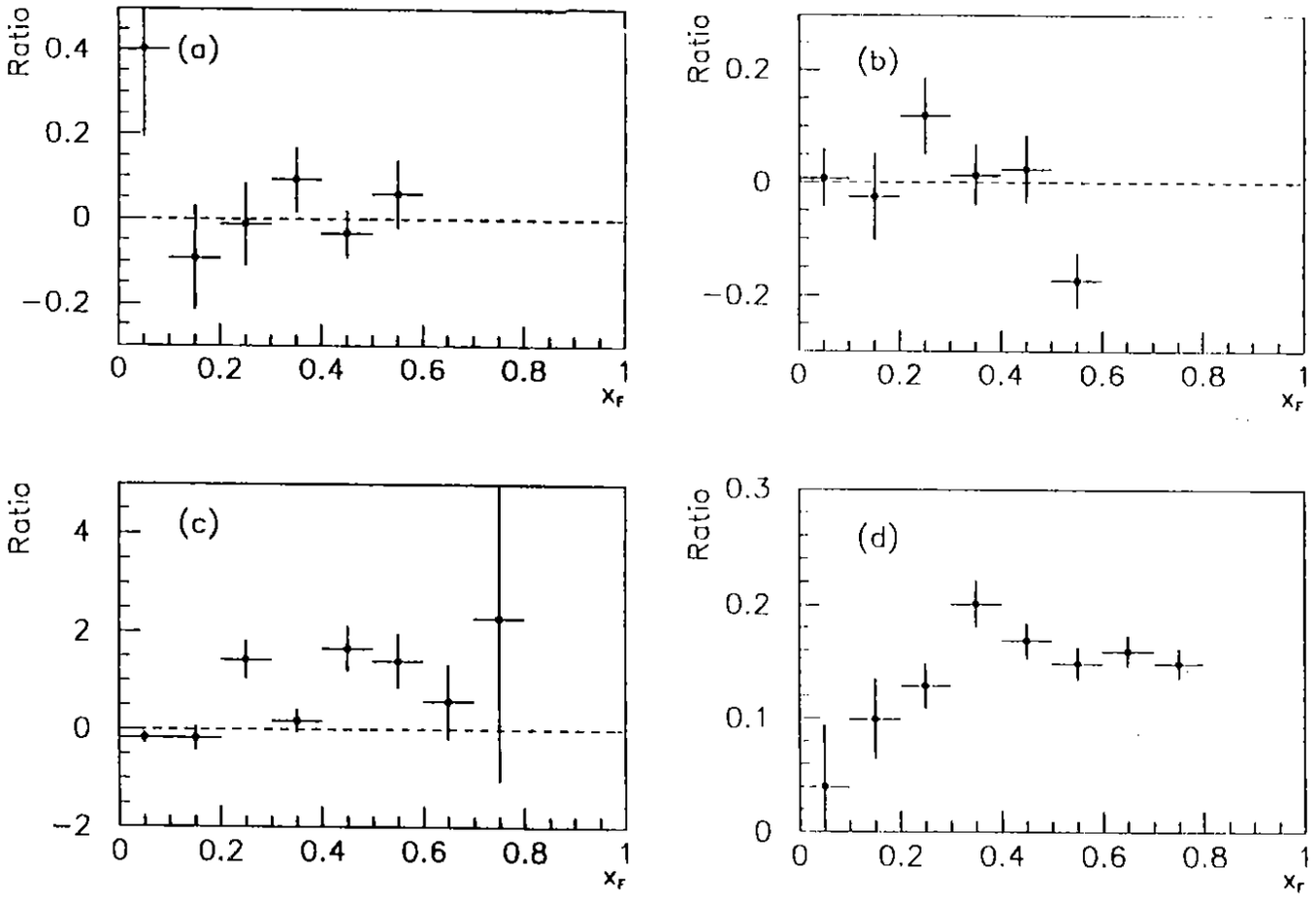

Figure 13: Ratios of structure functions: (a) (V(s)V)/(V(s)S), (b) (λS(s)V) / (λS(s)S+SS(s) from the pion, (c) (λS(s)V) / (λS(s)S+SS(s)) from the kaon, (d) (VS(s) from pion) / (V(s)S from kaon) .

CERN have been very generous in their support and this is most gratefully acknowledged.

References

[1] P.V. Chliapnikov et al.: Z. Phys. C12 (1982) 99

[2] E.A. de Wolf et al.: Z. Phys. C12 (1982) 105

[3] M. Barth et al.: Nucl. Phys. B223 (1983) 296

[4] H. Dijkstra et al.: Z. Phys. C31 (1986) 375

[5] S. Banerjee et al.: Z. Phys. C31 (1986) 401

[6] N.M. Agababyan et al.: Z. Phys. C41 (1989) 539

[7] H. Fawcett et al.: Z. Phys. C46 (1990) 513

[8] S.D. Drell, T. Yan, Ann. Phys.: 66 (1971) 578
M.B. Green, M. Jacob, P.V. Landshoff: Nuovo Cimento 29A (1975) 123
A. Donnachie, P.V.Landshoff: Nucl. Phys. B112 (1976) 233

[9] R.J. Apsimon et al.: Z. Phys. C53 (1992) 581

[10] A.B. Clegg: Z. Phys C55 (1992) 135

[11] R.J. Apsimon et al.: Nucl. Inst. Meth. A248 (1986) 76

[12] M. Baake et al.: Nucl. Inst. Meth. A281 (1989) 325

[13] R.J. Apsimon et al., Z. Phys. C52 (1991) 397

[14] R.J. Apsimon et al., Z. Phys. C43 (1989) 63

[15] J.C. Lassalle et al.: CERN-DD/EE/79-2 and Nucl. Instr. Meth. 176 (1980) 371

[16] H.U. Bengtsson, G. Ingelman, T. Sjöstrand, A. Weigend: CERN Pool Program W5035/W5045...W5048 (1987)

[17] G. Marchesini, B.R. Webber: CERN Pool Program W5037 (1989)

[18] Particle Data Group: Phys. Lett. B239 (1990)

[19] R.J. Apsimon et al.: Z. Phys. C56 (1992) 185

[20] F. James, M. Roos: CERN Pool Program D506 (1989)

[21] R.J. Apsimon et al.: Z. Phys. C46 (1990) 35

[22] M. Atkinson et al.: Z. Phys. C30 521 (1986)

[23] F.-D. Gebert: PhD thesis, University of Bonn (1992), BONN IR 92-40

[24] S.N. Ganguli, D.P. Roy: Phys. Rep. 67 (1980) 201

[25] H. Dijkstra et al.: Z. Phys. C31 (1986) 391

[26] H. Fawcett et al.: Z. Phys. C46 (1990) 521

[27] D. Aston et al.: Nucl. Phys B179 (1981) 215

[28] J. Morfin, W.K. Tung: Z. Phys. C52 (1991) 13

[29] M. Glück, E. Reya, A. Vogt: Z. Phys. C48 (1990) 471

[30] A. Donnachie, P.V. Landshoff: Z. Phys. in press

[31] J. Botts et al.: Phys. Lett. B304 (1993) 159